5-22-2009

Proceedings of the 38th Annual Biochemical Engineering Symposium

Matt J. Kipper
Colorado State University - Fort Collins

S. Ranil Wickramasinghe
Colorado State University - Fort Collins

Proceedings of the

38th Annual Biochemical Engineering Symposium

22-23 May 2009

Matt J. Kipper
S. Ranil Wickramasinghe
Editors

Department of Chemical and Biological Engineering
Colorado State University
Fort Collins, CO 80523-1370, USA

Proceedings of the 38th Annual Biochemical Engineering Symposium 22-23 May 2009

Matt J. Kipper
S. Ranil Wickramasinghe
Editors

Department of Chemical and Biological Engineering
Colorado State University
Fort Collins, CO 80523-1370, USA

Preface

The 38th Annual Biochemical Engineering Symposium was held at the Pingree Park Campus and Conference Center, Colorado State University, 22-23 May 2009. The following institutions were represented; Colorado State University, Iowa State University, Kansas State University and the South Dakota School of Mines. This Proceeding contains papers based on most of the oral presentations. The first symposium was first held in 1971. It has been held annually since then except for a one year break. The following institutions have hosted the symposium.

Colorado State University
Iowa State University
Kansas State University
South Dakota School of Mines and Technology
University of Colorado Boulder
University of Missouri Columbia
University of Nebraska-Lincoln
University of Oklahoma

The symposium aims to provide graduate students and occasional undergraduates experience at giving oral and poster presentations in public to their peers. This year's Proceedings begins with a review by Larry Erickson of the Biochemical Engineering Symposia that have been held over the years. Larry Erickson and Peter Rilley founded the Biochemical Engineering Symposium in 1971. We hope you enjoy reading the proceedings as much as we enjoyed listening to the talks. Finally we would like to invite all of you to the 39th Symposium to be hosted by Kansas State University in 2010.

Matt J. Kipper
S. Ranil Wickramasinghe
Editors
Department of Chemical and bio9logical Engineering
Colorado State University
Fort Collins, Co 80523-1370, USA
Telephone +1 970 491 5252

List of Participants

Colorado State University

Jorge Almodóvar
Soheil Boddohi
Matt Kipper
Xianghong Qian
Emily Stump
Xinying Wang
Ranil Wickramasinghe

Iowa State University
David Cantu
Brenda Carrillo-Conde
Yingfei Chen
Canan Marti
Mustafa Marti
Luis Petersen
Peter Reilly
Christopher Setina
Ryan Swanson
Quyen Truong

Kansas State University
Larry Erickson
Laurel Erickson

South Dakota School of Mines and Technology
Devon Burke
Brian Carter
Patrick Gilcrease

Contents

History of the Annual Biochemical Engineering Symposium

Larry E. Erickson
Department of Chemical Engineering
Kansas State University
Manhattan, Kansas 66506

The Annual Biochemical Engineering Symposium began in 1971, some years after teaching and research in biochemical engineering had become a part of a number of chemical engineering programs in the United States.

Biochemical engineering began to be a more significant part of chemical engineering research and education during and immediately after World War 2. Professor Elmer Gaden completed his Ph.D. research on oxygen transfer in fermentations during this period of time and began his career as a professor of chemical engineering with an emphasis on biochemical engineering (Hixon and Gaden, 1950). There were only a few faculty in chemical engineering departments during the period from 1950 - 1960 that were teaching biochemical engineering courses and conducting research in biochemical engineering. In 1959, sufficient interest and activity had developed in the field for a new journal, Biotechnology and Bioengineering to be founded (Humphrey, 1991). Elmer Gaden was one of the editors of the first volume; he soon became the sole editor. In 1965, Shuichi Aiba, Arthur Humphrey (a former graduate student of Gaden's), and Nancy Millis co-authored the first modern biochemical engineering textbook, Biochemical Engineering (Aiba et al., 1965). Professor Humphrey used his book for his course in Biochemical Engineering at the University of Pennsylvania, where Peter Reilly had received his Ph.D. and Larry Erickson conducted postdoctoral research.

In 1971 biochemical engineering instruction and research had become part of the chemical engineering activities at the University of Nebraska and Kansas State University, where Reilly and Erickson were young faculty members. They decided to begin an annual biochemical engineering symposium as part of their effort to mentor and educate the students who were studying in the field. The first annual biochemical engineering symposium was held at Kansas State on June 4, 1971 with 22 students and faculty from the University of Nebraska and Kansas State University attending. Peter Reilly, L.T. Fan, and Larry Erickson were the faculty that were present. Only 130 miles separated the two campuses and no overnight stay was necessary.

For the first four years, the Nebraska and Kansas State hosted the event in alternate years. After Peter Reilly moved to Iowa State University in 1974, the annual event continued with Iowa State becoming an active participant. The Sixth meeting was held in a hotel in Kansas City in conjunction with an AIChE meeting with Elmer Gaden attending. In 1977, Iowa State hosted the symposium in Ames, and Charles Dunlap and students from the University of Missouri-Columbia participated. In 1978, the meeting was held at Missouri-Columbia with Dunlap and George Preckshot hosting the event.

In 1979, students and faculty (Antonio Moreira and Vince Murphy) from Colorado State University participated for the first time with Kansas State as host. This greatly increased the geographical scope of the symposium. In 1981, Colorado State hosted the meeting and Moreira edited the proceedings. In 1982, the University of Arkansas participated for the first time; Ed Clausen attended from there and Kansas State was the host. In 1984, six universities participated with faculty and students from the University of Missouri-Rolla and Washington University attending. Oliver Sitton and Eric Dunlap were the faculty participants.

In 1985, the event was held on the Pingree Park campus of Colorado State; James Linden edited the proceedings and the University of Colorado participated for the first time (Rob Davis was the CU faculty member). In 1987, the University of Iowa participated and seven universities were represented. In 1988, Colorado hosted the meeting at the YMCA of the Rockies at Estes Park, and Rob Davis edited the proceedings. In 1990, Roger Harrison and students from the University of Oklahoma attended for the first time; Kansas State hosted with six universities participating.

Colorado State hosted the event in 1991 with seven universities present; Michael Meagher, who had participated earlier as a student at Colorado State and Iowa State, was present as a faculty member from Nebraska.

Kenneth Reardon edited the proceedings. In 1995, Marylee Southard and students from the University of Kansas attended for the first time with Missouri-Columbia as the host; Rakesh Bajpai edited the proceedings.

In 1997, Patrick Gilcrease, who had participated earlier as a Colorado State student, attended the meeting with students from the University of Wyoming. Colorado State hosted the meeting and Vince Murphy edited the proceedings. In 1999, Oklahoma State University and Rice University were represented with the Oklahoma as the host. In 2000, the event was held at the YMCA of the Rockies with Colorado as the host and Dhinakar Kompala edited the proceedings. After Gilcrease moved to South Dakota School of Mines and Technology, students and faculty from SDSMT began to attend the meetings, starting in 2002. In 2006, the meeting was held at the SDSMT and Gilcrease edited the proceedings.

Many different faculty have hosted the meeting and edited the proceedings. Peter Reilly has edited the proceedings 12 times; he has been a very strong advocate of the meetings. Fan and Erickson have edited the proceedings for the 10 meetings held at Kansas State. Rakesh Bajpai and Roger Harrison have each hosted and edited the proceedings three times. Six universities have participated in 10 or more of the meetings: Kansas State (38), Iowa State (34), Colorado State (25), Missouri-Columbia (19), Oklahoma (14), and Colorado (13).

Because of the increasing importance of biochemical engineering, many chemical engineering departments now have several faculty with interests in biochemical engineering. Bioseparations has become a more important part of biochemical engineering; Chuck Glatz and his students have attended several of the meetings, and they have added significantly to the bioseparations content of the meetings. The bioseparations book, coauthored by Harrision et al. (2003) benefited from the dialog that has taken place at the annual meetings (Harrison et al., 2003).

Today, many chemical engineering departments including those at Colorado State, Iowa State, Oklahoma, and SDSMT have added biological engineering or a closely related term to their department name. Kansas State has added a secondary major in Biological Engineering.

Graduate students are able to travel to national and international meetings because more funding is available for travel today than in earlier years. Interest and participation in the annual biochemical engineering symposium has decreased because of these factors.

The 2009 symposium hosted by Colorado State at their Pingree Park campus had the benefit of good leadership by Matt Kipper, who participated in earlier meetings while he was a student at Iowa State University. The 2010 meeting will be held at Kansas State University in order to take advantage of the central location offered by Kansas State.

References

1. Aiba, S., A.E. Humphrey, and N.F. Millis. 1965. Biochemical Engineering, Academic Press, New York.

2. Harrison, R.G. P. W. Todd, S.R. Rudge, and D. Petrides. 2003. Bioseparations Science and Engineering, Oxford University Press, New York.

3. Hixon, A. and E.L. Gaden. 1950. "Oxygen Transfer in Submerged Fermentation," Industrial and Engineering Chemistry 42: 1792.

4. Humphrey, A.E. 1991. "Elmer L. Gaden, Jr., Father of Biochemical Engineering," Biotechnology and Bioengineering, 37: 995-997.

Enhanced Solid-Liquid Clarification of Lignocellulosic Slurries Using Polyelectrolyte Flocculating Agents

Devon R. Burke, Jason Anderson, Patrick C. Gilcrease and Todd J. Menkhaus
South Dakota School of Mines and Technology, Department of Chemical and Biological Engineering, 501 East Saint Joseph St., Rapid City, SD 57701

1. Introduction

The United States currently imports over 10 million barrels per day of petroleum as a feedstock for fuels and chemicals [1]. However, environmental, economic, and national security concerns associated with petroleum have motivated research into alternative, renewable, domestic sources for fuels and chemicals [2]. Currently, ethanol is the primary alternative fuel source being evaluated as a replacement for gasoline.

The majority of ethanol production within the United States comes from the fermentation of glucose derived from corn starch. While the process of converting corn starch into fermentable sugars has been well developed, there are many potential drawbacks. For instance, bioethanol production consumes more than 12% of the corn produced in the United States [3]. This has led to higher costs for feed in the dairy, poultry, and livestock industries and has sparked debate over limiting subsidies for corn ethanol [4]. To help alleviate these concerns, other carbohydrate feedstocks are being considered.

Currently, different renewable lignocellulosic biomass sources (i.e., perennial grasses, woods, and cornstalks) are being tested to determine their viability as new, cost effective sources for fermentable sugars. Lignocellulosic materials are the most abundant renewable resource on earth, and new technologies are advancing their potential as an economical feedstock for fuel and chemical production [5]. Unfortunately, ethanol production from these materials has proven to be challenging because of the physio-chemical, structural, and compositional factors of the material. Compared to corn starch, cellulose is much more difficult to hydrolyze into glucose due to the recalcitrant nature of this polysaccharide and its associated biomass [6].

Lignocellulosic material is composed of three primary components: cellulose, hemicellulose, and lignin. The traditional process for breaking down lignocellulosic materials into fermentable sugars involves a pretreatment step to release cellulose/hemicellulose from the recalcitrant lignin sheath followed by enzymatic conversion of cellulose to glucose (Figure 1) for a separate hydrolysis and fermentation (SHF) process [7]. SHF utilizes separate steps for pretreatment, hydrolysis, and finally fermentation of the lignocellulosic material. Solid-liquid clarification can take place before and/or after the fermentation process.

Clarification is complicated when small low density particulate matter and colloidal materials are suspended in solution (as is the case with many lignocellulosic biomass processes). However, processes such as sedimentation, centrifugation, and filtration can be greatly improved through the use of flocculating agents. Flocculating agents are high molecular weight polymers that come in a variety of chemical compositions, concentrations, and charges; they are commonly used in the water treatment, biopharmaceutical, and papermill industries [10-14]. Generally these polymers are water soluble and are broadly characterized by their ionic nature: cationic, anionic, and non-ionic (neutral), and are referred to as polyelectrolytes [15]. By agglomerating suspended solids the flocculation process not only increases the size of the solids (making them more easily removed from solution), but also serves to scavenge very small particles that would normally be extremely difficult to remove [16-18].

Following efficient pretreatment and enzymatic hydrolysis steps, the slurry contains suspended solids that have a high percentage of lignin.. Though complex and undefined, the lignin structure of lignocellulosic biomass is highly branched and includes many exposed weak acid groups that are negatively charged [22]. It is hypothesized that these exposed charges will readily interact with charged surfaces of polyelectrolytes, causing flocculation and rapid removal of solids from solution. In addition, residual cellulose and/or hemicellulose remaining in the slurry following pretreatment and enzymatic hydrolysis will also contain exposed hydroxyl groups that could also interact with flocculants. For this project the primary goal was to evaluate and understand polyelectrolyte flocculation as a technique to improve the solid-liquid clarification of Ponderosa Pine hydrolyzate within a biorefinery system. Different polymers (cationic, anionic, and neutral) and clarification alternatives (centrifugation and filtration) were evaluated to determine optimal conditions and compare solid-liquid separation performance to non-flocculated slurries.

2. Materials and Methods

2.1 Preparation and Characterization of Pine Wood Hydrolysate

2.1.1 Pine Wood Hydrolysate

Ponderosa Pine sawdust from the Black Hills of South Dakota was used throughout the project and obtained from Baker Timber (Rockerville, SD). After removing all large contaminants (metal shaving, rocks, etc.), the material was dried by a two stage process. Wood was first dried in a fume hood operating at room temperature, and then in a 50 °C oven for 24 hours. The dried wood was then sieved to remove particles larger than 850 μm and stored in a sealed plastic vessel until further use. The moisture content of the dried wood was determined as discussed in Section 2.1.2.1.

Dilute acid pretreatment was completed in accordance with the National Renewable Energy Laboratory (NREL) Protocol LAP-007 [23,24] using a 4-L, high-pressure, high-temperature Parr® Reactor (Moline, IL). Two liters of slurry containing 10% w/w bone dry wood in 1% w/w sulfuric acid (prepared from concentrated sulfuric acid; Fisher, St. Louis, MO) was added to the glass-lined Parr Reactor containing cooling coils, followed by digestion at 160 °C (+/- 5°C) for 35 minutes (ramp-up to temperature set point took ~50 minutes, and cool down to room temperature took ~25 min). The reactor was agitated at 250 rpm with twin turbine blades.

Pretreated slurries were neutralized with concentrated ammonium hydroxide (14.5 M; Fisher, St. Louis, MO) from an initial pH of ~1 to a final pH of 5. Enzymatic hydrolysis was then completed in a 4-L reaction vessel agitated at 200 RPM and controlled at 50 °C. For this, Novozyme (Davis, CA) enzymes NS50010 (β-glucosidase) and NS50013 (endo-/exo-glucanase mixture) were each dosed to a concentration of 30 FPU/g cellulose (based on each enzyme having a manufacturer reported activity of 70 FPU/mL and the amount of cellulose determined by methods discussed in Section 2.1.2.2). Hydrolysis was allowed to progress for 72 hours and the pH was manually monitored and adjusted to pH 5.0 with sulfuric acid or ammonium hydroxide as needed. The final hydrolysate was stored at 4 °C until further testing and was utilized within two weeks or fresh material was prepared.

2.1.2 Analytical Methods

2.1.2.1 Moisture Content and Solids Analysis

The moisture content, percent total solids (TS), percent suspended solids (SS), and percent dissolved solids (DS) of the wood/slurry samples were determined using a modified

version of Standard Method 2540 for solids determinations within the water and wastewater industry using 2 g samples[25].

2.1.2.2 Compositional Analysis

The concentration (percentage) of hemicellulose, cellulose, lignin, and ash was estimated for the Ponderosa Pine wood using a modified version of NREL method LAP-014 [26]. Pine sawdust (0.03 g dried substrate) was added to a Hungate Tube (Fisher, St. Louis, MO) along with 0.3 mL of concentrated (72 wt%) sulfuric acid. Tubes were placed horizontally in an incubator at 30 °C for 2 hours with low speed 40 rpm mixing. After removing the tubes, 8.4 mL of distilled water was added to each tube, resealed, and autoclaved for 15 minutes at 121 °C. Tubes were quickly cooled and neutralized with 0.35 g of solid calcium carbonate (Fisher, St. Louis, MO). Samples were then filtered with a 0.2μm nylon syringe filter into HPLC vials for analysis (Section 2.1.2.3). As an estimate, the percentage of cellulose was calculated from the glucose concentration, while hemicellulose was estimated from the xylose, mannose, galactose, and arabinose concentrations, and the remainder of the wood was assumed to be lignin/ash. Control samples of pure glucose and xylose were also prepared to account for any degradation compounds produced. The volume of water in the wood sample, as well as additional volume of water, acid, and base during the analysis was explicitly accounted for in the calculations. Analyses were completed throughout the duration of the project to ensure consistent composition of the feedstock. It is know that less than 3% w/w of the hemicellulose in pine woods result in glucose as the monomeric sugar [27], and thus it would be reasonable to correlate the glucose concentration to initial cellulose present.

2.1.2.3 Sugars Analysis

The concentrations of soluble compounds in the generated experimental slurries were quantified using High Pressure Liquid Chromatography (HPLC). Total sugars (a combined peak containing all unseparated sugars), acetic acid, furfural, hydroxymethyl furfural, and ethanol were separated using a Biorad Aminex® HPX-87H column. A "carbohydrate" column (Biorad HPX-87P) was also used to further separate the sugars into the specific monomeric forms (glucose, xylose, mannose, galactose, and arabinose). The appropriate column was installed into a Beckman Coulter® HPLC system, which included: System Gold ® 509 Autosampler, 125 Solvent Module Pump, and 32 Karat Software. A Jasco intelligent refractive index (RI) detector (Model RI-1530) was used in the system, as well as a Timberline Instruments® column heater (Model 105). The mobile phase used in the system was 5mM H_2SO_4 prepared with 0.2 μm filtered distilled water, and the column operated at a temperature of 60 °C, with a constant flow rate of 0.2 mL/min.

2.1.2.4 Zeta Potential

The zeta potential of wood slurries and flocculated solids was measured as an estimate of surface charge. For this, a Zeta Reader Mark 21 from Zeta Potential Instruments (Bedminster, NJ) was used. Samples were diluted with water to obtain the necessary concentration of approximately 100 – 1000 mg suspended solids/L of solution prior to reading. The pH was not affected by dilution. A minimum of 10 readings per sample were made at 100 V and results were averaged. Due to the large size of some flocs that clogged the sample port, the zeta potential was measured on smaller solids remaining after a brief (30 sec) settling. This method has been shown to represent the zeta potential of solids in the floc [20].

2.2 Flocculation

Polyelectrolyte flocculants were received from Kemira North America (Mobile, AL), with different charge, molecular weight, and charge density as shown in Table 1. All polymers

were diluted to a working solution concentration of 10 g/L in water and adjusted to pH 5.0 with small amounts (<0.1% of total volume) of sulfuric acid or ammonium hydroxide, prior to flocculation experiments. Stored pine hydrolysate following enzymatic digestion was thoroughly mixed and a subsample was removed and allowed to warm to room temperature (~22°C); all tests were completed with no additional heating or cooling. The concentrated polymer stock (10 g/L) solution was added directly to the slurry in required amounts to provide the desired final concentration of polymer, and gently mixed for a minimum of 5 minutes before performing any analyses.

2.3 Centrifugation Tests

Flocculation was performed with 25 mL of slurry in a 50 mL centrifuge tube. The largest volume of polymer added was 2.78 mL, and in all cases the additional volume was explicitly accounted for in solids and sugar recovery calculations. The pH of the hydrolysate was not affected by the addition of these amounts of polymer. The sample tubes were then placed into a JA-20 rotor and centrifuged in a Beckman-Coulter J2-HS centrifuge (Fullerton, CA) at rotational velocities of 1000, 1500, 2500, and 3500 RPM (corresponding to 121, 272, 755, and 1480 x g) for 5 min.

2.4 Filtration Tests and Particle Size Distribution

The particle size distribution of the hydrolysates was determined using a step-wise wet sieving approach. Following addition of the flocculant (Section 2.2) 25 mL of the resulting slurry was filtered using a normal flow (dead end) device (Nalgene, 250 mL capacity filtration assembly, Sigma Aldrich, St. Louis, MO), with a 47 mm diameter pre-weighed brass filter, with size cutoff of 595µm (standard mesh #30; Cole Parmer, Vernon Hills, IL) and 1 atm of vacuum. The slurry was gently mixed to discourage cake formation, and solids were thoroughly washed to ensure that all solids <595 µm passed through the filter. The procedure was then repeated using the filtrate as the sample and a mesh opening of 250µm (standard mesh #60). This process continued using size cutoffs of 149µm (standard mesh #100) and 63µm (standard mesh #230). The screens were then placed in an oven at 103 °C for a minimum of 24 hours. The final dry weight of suspended solids captured by each filter was then calculated by re-weighing the brass mesh with dry solids. The final filtrate from the 63µm mesh was also analyzed for total solids, total suspended solids, and total dissolved solids.

For evaluation of the filtration process, the same apparatus was utilized, but only the 63µm mesh was evaluated, and 500 mL of slurry was directly filtered. Filtrate was collected in a graduated cylinder and volume was measured at discrete times. Pressure was maintained at 1.0 atm vacuum for the duration of the analysis, and only course mixing above the filter surface was allowed (no scraping the surface, only the bulk slurry above the surface). This setup was made to mimic an industrial scale rotary vacuum or vacuum belt operation.

2.5 Fermentations

Shake flask fermentations were completed to assess the effect of small concentrations of polyelectrolyte on the ability of a commercial yeast to produce ethanol. The yeast strain used in the research was the D_5A strain of *Saccharomyces cerevisiae*, which was obtained from NREL. The D_5A strain was capable of fermenting only glucose into ethanol. Fresh cultures were prepared by adding 2.5 mL frozen inoculum to 25 mL of yeast peptone dextrose (YPD) media in a 100 mL baffled shake flask. YPD media contained 10 g/L yeast extract, 20 g/L peptone, and 20 g/L glucose; the media was pH adjusted to 5.0 using H_2SO_4 and NH_4OH. The culture was allowed to grow for 16 hours at 37 °C and 250 RPM . This starter culture was then diluted with 250 mL of YPD and again allowed to grow for 16 hours at 37 °C and 250 RPM in a 1 L baffled

shake flask. Modified YPD media was prepared with 0, 100, 200, 400, 750, and 1000 mg of C-1592/L of media. The growing culture (40 mL) was then added to 400 mL of the modified media containing different concentrations of C-1592 in 2 L shake flasks, and allowed to grow at 37 °C and 250 RPM. All fermentations were conducted anaerobically using stopper sealed flasks with a syringe inserted for off-gas release. Samples were taken every hour to analyze for glucose consumption, cell growth, and ethanol production.

3. Theory

Centrifugation is one of the most common separation processes to remove suspended solids from solution. Centrifugal forces are used to enhance gravitational acceleration with the intent of increasing particle sedimentation velocities [28]. The acceleration forces solids particles toward the bottom or outside of the rotor or bowl, while the liquid supernatant remains on the top and is collected as clarified solution.

In its simplest form, for a standard batch laboratory centrifuge, the "g" force applied to the rotor or bowl can be calculated from the bowl/rotor radius and the revolutions per minute (RPMs) at which the bowl is rotating. Equation 1, shows an equation for Gt, or "g" forces multiplied by unit time for the separation.

$$Gt = \frac{\omega^2 * R_o}{g} * t \qquad \text{Equation 1}$$

Where ω is the rotor speed, R_o is the average rotor radius, g is the gravitational constant, and t is the time.

As the rotor speed (RPM), rotor size, or time of separation is increased, so does the total amount of energy applied to the system. Likewise, as Gt increases, so should the solid-liquid separation; as more power is applied, or more time is allowed for the separation, more solids should be pulled out of solution. Higher Gt also helps accomplish the task of removing smaller suspended solids that would not be removed under lower force.

The sigma equation, as shown in Equation 2 for an industrial scroll decanter, and Equation 3 for a batch centrifuge, is another means of describing centrifuge properties and operation.

$$\Sigma_{industrial} = \frac{\omega^2 \pi b 2r^2}{g} \qquad \text{Equation 2}$$

Where r is the rotor radius and b is the rotor length.

$$\Sigma_{lab} = \frac{\omega^2 V}{\ln\left[\frac{2r_2}{r_2 + r_1}\right] 2g} \qquad \text{Equation 3}$$

Where V is the volume of slurry, r_1 is radius to liquid level, and r_2 is the radius to bottom of centrifuge bottle.

The sigma factor calculates the gravitational "settling area" from the characteristics of a corresponding centrifuge [8]. It can be used to relate the performance of one centrifuge to that of another through Equation 4. By determining a required lab sigma factor to accomplish a desired separation with a small scale centrifuge, Equation 4 can be used to calculate the allowed flow

rate for a given industrial centrifuge. Alternatively, if a required flow rate is known, the centrifuge properties for the industrial process can be determined through sigma industrial.

$$\frac{Q_{industrial}}{\Sigma_{industrial}} = \frac{V}{t\Sigma_{lab}} \qquad \text{Equation 4}$$

Filtration is also commonly used throughout industry to remove solids from suspensions. Optimum filtration is achieved by maximizing the flux of solvent through the filter mesh. Equation 5 shows the basic filtration flux equation.

$$Flux = \frac{Volume}{Time * Area} = \frac{dV}{dt} * \frac{1}{A} \qquad \text{Equation 5}$$

Within a laboratory setting, collecting filtrate volume (V) as a function of time (t), for a given membrane area (A) is the most practical means of obtaining flux data, which can be modeled as flow through a porous bed of solids by Darcy's Law (Equation 6).

$$\frac{1}{A} * \frac{dV}{dt} = \frac{\Delta P}{\mu\left(\frac{\alpha * c_s * V}{A} + R_m\right)} \qquad \text{Equation 6}$$

Where ΔP is the pressure differential across the filter, μ is the filtrate viscosity, α is the specific cake resistance, c_s is the solids concentration in suspension, and R_m is the filter medium resistance.

The right-hand side of Equation 6 shows that the volumetic flowrate of liquid through the filter should increase linearly with the applied differential pressure across the filter membrane, but decrease due to resistance from the membrane and cake. Flux will also continually decline as more solids build up on the surface of the filter in proportion to the specific cake resistance. Solving the differential equation shows that by plotting tA/V versus V/A, the slope of the plot can be used to determine α, while the y-intercept can be used to calculate R_m [8,9].

4. Results and Discussion

4.1 Initial Assessment of Flocculation

The bone dry composition of Ponderosa Pine used for all experiments was found to be (average ± standard deviation of 4 samples): 40% w/w cellulose (±5%), 18% hemicellulose (±4%), and 42% lignin/ash (±5%). This is in good agreement with composition of other pine woods reported in the literature [27,29,30]. Following pretreatment and enzymatic hydrolysis, the solids content of the resulting slurry (average of 4 preparations) contained 5.5% w/w (±0.2%) suspended solids and 4.8% w/w (±0.3%) dissolved solids at pH 5.0. The liquid contained 26.3 g/L glucose (±2.8 g/L), 5.3 g/L xylose (±1.2 g/L), 8.1 g/L mannose (±1.9 g/L), 7.7 g/L acetic acid (± 1.7 g/L), 0.8 g/L hydroxymethyl furfural (±0.3 g/L) (HMF), and 1.1 g/L furfural (±0.3 g/L). The average theoretical cellulose conversion to glucose was 59-73%. This indicated that in addition to lignin, there was still a significant proportion of residual cellulose and hemicellulose in polymeric form that contributed to the suspended solids fraction. Assuming the average conversion of cellulose to glucose and HMF was 68%, and the conversion of hemicellulose to sugars and furfural was 79%, with no digestion of lignin, the suspended solids contained (mass basis) approximately 22% cellulose (or smaller non-monomeric subunits such as cellobiose), 6% hemicellulose (or smaller non-monomeric subunits), and 72% lignin.

Numerous polymers with different properties were initially tested to determine their potential as a suitable flocculating agent (Table 1). Flocculant was continually added to the biomass slurry in increments of 20 mg polymer/L slurry, from 0 – 5000 mg/L. From this initial analysis, Kemira Superfloc C1592 showed the strongest performance by allowing the largest flocs to form that were quickly settled out of solution (Figure 3). Kemira C1594 and C1598 also showed an ability to flocculate solids, but the flocs produced were visually much smaller. C1592, C1594, and C1598 were all cationic polyacrylamides, sharing the same chemical structure and molecular weight of $4x10^6$. The polymers varied in their percent mole charge, or effective charge density; 10, 20, and 40% for C1592, C1594, and C1598, respectively. For the higher charge density of C1594 and C1598 under similar volumetric dosages to C1592, the resulting charge difference between solids and flocculant was probably too large, and ended up producing some solids repulsion effects; it is likely that the positive charge of the polymer surpassed the charge neutralization phase (discussed below) resulting in smaller flocs.

A zeta potential analysis was performed on suspended solids to determine average particle surface charge. A representative zeta potential was determined to be -22.72 mV (±3.83 mV) for a Parr pretreated and enzymatically digested hydrolyzate. The results confirmed the theory that the suspended solids in the experimental slurries had negative surface charge and floucculated well to cationic polyelectrolyte polymers; electrostatic ionic interactions between suspended and colloidal substances, like hemicellulose, cellulose and lignin compounds, and cationic polyelectrolytes have been observed in previous studies from the paper mill industry [30]. Zeta potential measurements of the optimum flocculated particles using C1592 were not possible because the particle size of the flocs was too large for the instrument. However, assessment of the smaller flocs formed with C1494 and C1598 showed that the zeta potential was quickly converted from negative to positive even at very low dosages with these higher charge density polymers, and a likely explanation for the greater dispersion observed.

Particle size distributions for wet suspended solids within the hydrolyzate, and for flocculated hydrolyzate at different concentrations of C1592 polyelectrolyte, show the dramatic effect that the polymer has on size distribution (Figure 4). The largest particles increase from ~15% of the total solid mass to almost 60% with the addition of 1000 mg polymer/L slurry. In addition, the cumulative percentage of small particles (e.g., those <250μm that are most difficult to remove from suspension), is reduced from 57% in the unflocculated sample to 6% with 1000 mg polymer/L. Also of note is that polymer concentrations higher and lower than 1000 mg/L both cause flocculation, and a corresponding increase in the percentage of larger particle size fractions, but the maximal benefit is seen at the intermediate dosages. The highest concentration tested actually led to a reversal of flocculation and even though it contained a significantly higher percentage of the largest solids, it also had nearly as many smaller particles as the un-flocculated sample. Finally, comparing the three intermediate polymer dosages (100, 500, and 1000 mg/L), they were all very similar. The 1000 mg/L dose provided the highest percentage of larger particles, but the 100 mg/L dose actually had the lowest percentage of the smallest particles <63μm.

4.2 Centrifugation Analysis

Centrifugation analysis as a solid-liquid separation operation was evaluated with the Ponderosa Pine hydrolyzate and C1592 polyelectrolyte flocculating agent. Varying concentrations of polymer along different centrifugal energy inputs (in the form of higher rotational velocities or centrifugation times) were investigated (Figure 5). Solids cake formed at low Gt values and/or low polymer concentrations were easily disrupted and caused greater error

in analysis of these samples (upper left of Figure 5). Higher Gt values and/or higher polymer concentrations provided much more stable solid pellets after centrifugation. It was also evident that by increasing the polymer dosage from 0 mg/L to 1000 mg/L the resulting centrate was more highly clarified at a given Gt value; thus, the flocculation process was capable of producing a centrate with a lower concentration of suspended solids at lower energy inputs. However, adding too much polymer (5000 mg/L) resulted in the solids re-dispersing, which were again more difficult to remove from solution.

At an industrial scale, the benefits of flocculation can be quantified by comparing the operational flow rates achievable for a desired degree of clarity when using an industrial scroll decanter centrifuge. For this analysis, a clarity value of 0.7% w/w suspended solids was chosen as the target. Then, a sigma factor of 0.065 m^2 was calculated from Equation 4 for the lab centrifuge operating at 1000 RPM. Similarly, an industrial centrifuge sigma factor of 2200 m^2 was calculated using Equation 3 for an Alfa Laval Model SG2-400 decanter centrifuge (Alfa Laval, Richmond, VA). Using the required centrifugation time of 5 minutes with 1000 mg polymer/L and 61 minutes for the no flocculant case, the anticipated flow rate with the industrial centrifuge was calculated from Equation 5. To obtain 0.7% w/w suspended solids in the centrate of an industrial centrifuge, only 1500 L/h could be processed without flocculant, while 18000 L/h could be processed with the aid of polyelectrolyte, a 12-fold improvement in throughput.

While clarity is one important performance indicator, the solid-liquid separation process should also allow for high sugars recovery in the centrate while simultaneously producing a relatively dry solids cake. Unfortunately, while the 500 mg/L and 1000 mg/L dosages optimize solids removal, a greater percentage of sugar-rich liquid was retained with the solids at these concentrations. This resulted in lower total recovery of sugars (Figure 6) and higher moisture content (lower solids percentage) in the cake (Figure 7) for higher concentrations of polyelectrolyte. The aqueous sugars concentrations for all samples evaluated (pre-clarification, non-flocculated, and flocculated) were within the error of the HPLC (±5%); thus, the loss of sugars was strictly from liquid being absorbed by the hydrophilic polymer. However, at 100 mg polymer/L, flocculation allowed for enhanced solids removal from the centrate while minimizing liquid retention. This indicated that an optimum could be achieved where large, porous flocs were formed without additional polymer acting as a sponge to remove sugar-rich liquid.

As a final performance measure, combining clarity and sugars recovery, the ratio of sugars to suspended solids in the centrate was calculated (Table 2). Ideally, the concentration of sugars would remain high and the concentration of suspended solids low. This would then allow for sugars concentrating operations (i.e., reverse osmosis or evaporation) to be completed with the least amount of fouling to membrane or evaporator surfaces. With this in mind, intermediate polymer concentrations (500 and 1000 mg/L) and higher Gt values provided the highest ratio of sugars to suspended solids.

4.3 Filtration

A simulated rotary vacuum filtration process was performed on both unflocculated and flocculated hydrolyzate using a 63 μm mesh. Flocculation was performed with 100 mg/L C1592 because centrifugation results showed that this dosage allowed for easy floc removal with minimal liquid retention. The liquid flux for the flocculated sample was approximately 40-times higher than for the unflocculated trial (Figure 8). Liquid from the flocculated sample drained through the mesh and porous flocs with very little resistance. Final sugar recovery in the filtrate was 84% with flocculant and 82% without flocculant. Much like centrifugation, the loss was due to liquid retained within the solid cake rather than adsorption to the polymer. It is important to

note the sugar recovery was ~10-20% higher using vacuum filtration as the clarification operation when compared to centrifugation (Figure 6). The corresponding total solids percentage in the filtration cake was 23.9% (±1.2%) for the unflocculated sample and 25.5% (±1.2%) for 100 mg/L sample; both significantly higher than the centrifugation results (Figure 7). Higher sugar recoveries (>90%) were achieved by washing the solids cake with water at 10% of the original slurry volume.

The mesh filter itself was found to be the dominant resistance to flow for the flocculated sample, with an R_m value calculated from the intercept of Figure 9 of 2.5×10^{10}m, while the specific cake resistance (α, calculated from the slope of Figure 9) was only 1.6×10^{8} m/kg. On the other hand, for the unflocculated sample, the cake resistance was more than 3 orders of magnitude higher than the flocculated sample with an α value of 2.1×10^{11} m/kg, as calculated from Figure 10. Similarly, it was speculated that the pores of the mesh became immediately clogged by particulates in the unflocculated sample, resulting in a mesh resistance of 4.0×10^{11} m.

Finally, the theoretical ratio of sugars concentration to suspended solids concentration for filtration operations with different mesh size openings was determined using particle size distribution data. For this, it was assumed that all particles larger than a given mesh size would be retained by that mesh. It was found that the optimal clarity was achieved with the 100 mg/L dosage and smallest screen (Table 3). This was not surprising due to the 100 mg polymer/L sample containing the lowest percentage of small particulates (Figure 3). The theoretical exercise matched two select points (0 and 100 mg/L with 63 μm mesh) where the actual filtration of total slurry was evaluated (as opposed to the sequential filtration used during particle size analysis). Interestingly, comparing Table 2 and Table 3, the results indicated that the highest Gt value used during centrifugation may have removed particles slightly larger than 63μm, leaving a slightly higher percentage of suspended fine solids in solution. Alternatively, the cake formed during filtration may have acted as a prefilter to the mesh capturing smaller particles.

4.4 Fermentations with C1592

From a cost standpoint, it would be desirable to use a low of concentration of polyelectrolyte. Lower dosages would also reduce concerns regarding downstream operations, as residual polymer could lead to increased viscosity or toxicity to fermentation organisms. While polyelectrolytes are used in many industries where human and animal health is monitored (i.e., biopharmaceutical, waste water treatment, and food and beverage processes), and are generally regarded as safe [29], there is still the possibility that residual polyelectrolye may be toxic to the organism or flocculate it. With this in mind, controlled fermentations were completed to evaluate increasing levels of C1592. The concentrations found to be effective at flocculating pine solids were relatively low compared to other applications, where concentrations can be an order of magnitude higher [31 – 34]. Additionaly, the concentration of polyelectrolyte remaining in solution after flocculation would be significantly less than the initial value. Nonetheless, we evaluated fermentations at C1592 concentrations up to 1000 mg/L, and found that no significant difference in cell growth (data not shown), glucose consumption, or ethanol production was observed (Figure 11). No discernable trends emerged from the data and all samples for a time point were within the error of the HPLC instrument (~5%).

5. Conclusions

Polyelectrolyte flocculating agents can be used to enhance the solid-liquid clarification of lignocellulosic biomass hydrolyzates. Due to the negative zeta potential of Ponderosa Pine

solids following pretreatment and enzymatic hydrolysis, primarily lignin, cationic polymers provided the largest flocs that quickly settled out of solution. Adding flocculant up to 1000 mg/L created larger flocs. However, a higher dosage (5000 mg/L) resulted in solids re-dispersing into solution. The addition of 100 mg/L of Kemira polyelectrolyte C1592 showed optimal supernatant clarity and sugar recovery capabilities. It was predicted that a greater than 12-fold improvement in throughput with a scroll decanting centrifuge could be obtained by using this flocculant, or that approximately 40-fold higher flux could be obtained for a vacuum filtration operation. Overall, the percentage of suspended solids remaining following either centrifugation or filtration was at least 10-times lower with the aid of the flocculant. Addition of the polymer to a standard *Saccharomyces cerevisiae* fermentation at levels up to 1000 mg/L did not affect culture growth or ethanol production.

6. Acknowledgements

Funding for this work was provided by the National Research Initiative of the USDA Cooperative State Research, Education, and Extension Service, Grant Number 2007-35504-18344 and the South Dakota Center for Bioprocessing Research and Development. The authors also acknowledge the donation of polyelectrolytes by Kemira North America (Mobile, AL).

References

1. Department of Energy, Energy Information Administration. Petroleum Statistics. http://www.eia.doe.gov/oil_gas/petroleum/info_glance/petroleum.html
2. Mosier, N., Wyman, C., & Dale, B. (2005). Features of promising technologies for pretreatment of lignocellulosic biomass. *Biores. Tech.*, 96(6), 673-686.
3. Yang, S.-T. (2007). *Bioprocessing for value-added products from renewable resources - New technologies and applications.* The Netherlands: Elsevier.
4. Tilman, D., & Hill, J. (2007, March 25). Corn can't solve our problem. *The Washington Post*, p. B01.
5. Lynd, L., van Zyl, W., & McBride, J. (2005). Consolidated bioprocessing of cellulosic biomass: an update. *Curr. Op. Biotech.*, 16, 577-583.
6. Laureno-Perez, L., Teymouri, F., Alizadeh, H., and Dale, B.E. (2005). Understanding factors that limit enzymatic hydrolysis of biomass. *App. Biochem. Biotech.*, 121-124: 1081 – 1099.
7. Olofsson, K., Bertilsson, M., & Lidén, G. (2008). A short review on SSF – an interesting process option for ethanol production from lignocellulosic feedstocks. *Biotech. Biofuels 1:7*.
8. Geankoplis, J. C. (2003). *Transport Processes and Separation Process Principles.* Upper Saddle River, NJ: Prentice Hall.
9. Harrison, R.G., Todd, P., Rudge, S.R., Petrides, D.P., 2003. Bioseparations Science and Engineering, first edition. Oxford University Press: New York.
10. Metes, A., Koprivanac, N., & Glasnovic, A. (2000). Flocculation as a treatment method for printing ink wastewater. *Water Env. Rsch.*, 72, 680-688.
11. Ravnjak, D., Fuente, E., Negro, C., & Blanco, A. (2006). Flocculation of pulp fractions induced by fluorescently - labelled PDADMAC. *Cellulose Chem. Tech.*, 40, 77-85.
12. Miyanishi, T., Shigeru, M., 1997. Optimizing flocculation and drainage for microparticle systems by controlling zeta potential. *Tappi J.*, 80(1): 262 – 270.
13. Britt, K. W., & Unbehend, J. E. (1985). Water removal during paper formation. *Tappi J.*, 68, 104-107.

14. Menkhaus, T.J., Eriksson, S.U., Whitson, P.B., Glatz, C.E., 2002. Host selection as a downstream strategy: Polyelectrolyte precipitation of beta-glucuronidase from plant extracts. *Biotechnol. Bioeng*, 77, 148-154.
15. Bolto, B., & Gregory, J. (2007). Organic polyelectrolytes in water treatment. *Water Rsch.*, 41, 2301-2324.
16. Galbe, M., Pilcher, L., & Roslander, C. (n.d.). Separation of Solid Residues after SSF and SHF in Fuel Ethanol Production from Spruce. *Dept. of Chemical Engineering 1, Lund University* .
17. Wickramasinghe, S., Han, B., & Akeprathumchai, S. (2004). Improved permeate flux by flocculation of biological feeds: comparison between theory and experiment. *J. Memb. Sci.* 242, 57-71.
18. Kim, J.-S., Akeprathumchai, S., & Wickramasinghe, S. (2001). Flocculation to enhance microfiltration. *J. of Memb. Sci.* 182 , 161-172.
19. Hubbe, M. A. (2007). Flocculation and redispersion of cellulosic fiber suspensions: A review of effects of hydrodynamic shear and polyelectrolytes. *BioResources,* 2 (2) , 296-331.
20. Pearson, C. R., Heng, M., Gebert, M., & Glatz, C. E. (2004). Zeta Potential as a Measure of Polyelectrolyte Flocculation and the Effect of Polymer Dosing Conditions on Cell Removal From Fermentation Broth. *Biotech. Bioeng.*, 87, (1) , 54-60.
21. Eriksson, L. (1987). Conditioning of biological sludges with cationic polyelectrolytes. *Water Sci. Tech.,* 19, 859-868.
22. Baptista, C., Robert, D., Duarte, A.P (2005). Effect of pulping conditions on lignin structure from maritime pine kraft pulps. *Chem. Eng. J.,* 121(2-3), 153-158.
23. Hayward, T. K., Combs, N. S., Schmidt, S. L., & Philippidis, G. P. (1995, May 31). SSF Experimental Protocols: Lignocellulosic Biomass Hydrolysis and Fermentation. *Laboratory Analytical Procedure (LAP) LAP-008.* NREL.
24. Stenberg, K., Bollók, M., Réczey, K., Galbe, M., & Zacchi, G. (2000). Effect of substrate and cellulase concentration on simultaneous saccharification and fermentation of steam-pretreated softwood for ethanol production. *Biotech. Bioeng.,* 68, 204-210.
25. Clescerl, Leonore S.(Editor), Greenberg, Arnold E.(Editor), Eaton, Andrew D. (Editor), 1998. *Standard Methods for the Examination of Water and Wastewater* (20th ed.) American Public Health Association, Washington, DC.
26. Ruiz, R., & Ehrman, T. (1996, August 12). Dilute acid hyrolysis procedure for determination of total sugars in the liquid fraction of process samples. *Laboratory Analytical Procedure (LAP) LAP-014* . NREL.
27. Sjostrom, E., *Wood Chemistry. Fundamentals and Applications.* Second edition, 1993, San Diego: Academic press.
28. Van Der Linden, J. P. (1987, February 5). Liquid-liquid separation in disk-stack centrifuges. *Doctorial Dissertation.* Netherlands: Bibliotheek Technical University.
29. Pan, X., Xie, D., Yu, R.W., Saddler, J.N. (2008). The bioconversion of mountain pine beetle-killed lodgepole pine to fuel ethanol using the organosolv process. *Biotech. Bioeng.,* 101(1), 39 – 48.
30. Kumar, A. (2009). A conceptual comparison of bioenergy options for using mountain pine beetle infested wood in Western Canada. *Biores. Techn.*, 100, 387 – 399.
31. Dunham, A. J., Tubergen, K. R., Govoni, S. T., & Alfano, J. C. (2000). The effects of dissolved and colloidal substances on flocculation of mechanical pulps. *Pulp Paper Sci.,* 26 , 95-101.

32. Cartier, S., Tatoud, L., Theoleyre, M.A., Decloux, M. (1997). Sugar refining processes by coupling flocculation and crossflow filtration. *J. Food Eng.*, 32(2): 155 – 166.
33. Aspelund, M.T.; Rozeboom, G.; Heng, M.; Glatz, C.E. (2008). Improving permeate flux and product transmission in the microfiltration of a bacterial cell suspension by flocculation with cationic polyelectrolytes. *J. Memb. Sci.*, 324(1+2), 198-208.
34. Radoiu, M.T., Martin, D.I., Calinescu, I., Iovu, H. (2004). Preparation of Polyelectrolytes for Wastewater Treatment. *J. Haz. Mat.*, 106(1): 27 – 37.
35. Strand, S.P., Kjell, M.V., Ostgaard, K. (2003). Interactions between chitosans and bacterial suspensions: Adsorption and flocculation. *Colloids and Surf. B*, 27, 71-81.

Table 1: Properties and qualititative observations of polyelectrolytes evaluated for flocculation of pine wood hydrolyzate solids.

Polymer (Kemira)	Molecular Weight	mol% charge	Charge	Qualitative Observations
130 GVHRS	30-35x10^6	30%	Anionic	Minor solid fines flocculation
140 GVHRS	30-35x10^6	40%	Anionic	Minor solid fines flocculation
A1883 RS	15-18x10^6	30%	Anionic	Minor solid fines flocculation
A1849 RS	15-18x10^6	3%	Anionic	Minor solid fines flocculation
N1986	15-18x10^6	0%	Neutral	Minor solid fines flocculation
C1592	4x10^6	10%	Cationic	Large flocs, rapid settling
C1594	4x10^6	20%	Cationic	Medium-sized flocs
C1598	4x10^6	40%	Cationic	Medium-sized flocs

Table 2: The ratio of total sugars concentration (g/g) to suspended solids (SS) concentration (g/g) following centrifugal clarification at different Gt and polymer dosage values. All values represent the average of 2 samples with less than 5% difference.

*Gt (g*min)* / Sugars/SS	*Polymer Concentration mg/L*				
	0	***100***	***500***	***1000***	***5000***
604	1.2	2.4	5.4	6.6	1.8
1360	1.6	3.3	11	13	2.5
3777	1.9	77	80	89	3.8
7402	6.3	519	476	453	20

Table 3: The ratio of total sugars concentration (g/g) to suspended solids (SS) concentration (g/g) following filtration clarification with different size cutoffs and polymer dosage values. All values are hypothetical based on particle size distribution analysis except for the 63μm filter using 0 and 100 mg/L dosages with values shown in parentheses taken directly from filtration experiments. All values represent the average of 2 samples with less than 5% difference.

Filter Cutoff (μm) / Sugars/SS	*Polymer Concentration mg/L*				
	0	***100***	***500***	***1000***	***5000***
595	1.6	2.7	3.0	3.2	2.0
250	2.3	7.3	16	21	3.4
149	5.3	46	33	36	7.1
63	78 (82)	764 (781)	509	478	80

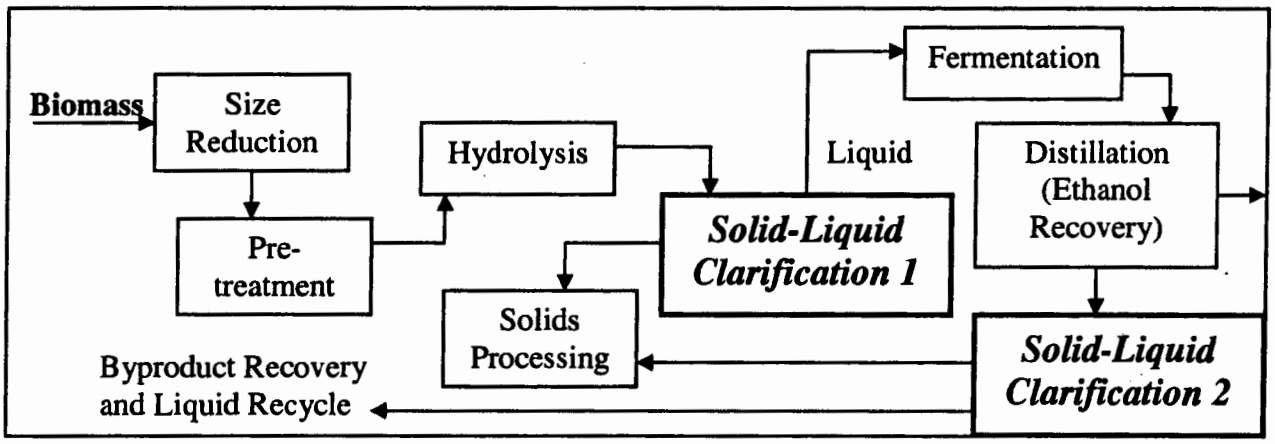

Figure 1: Schematic of separate hydrolysis and fermentation process for the conversion of lignocellulosic biomass into ethanol.

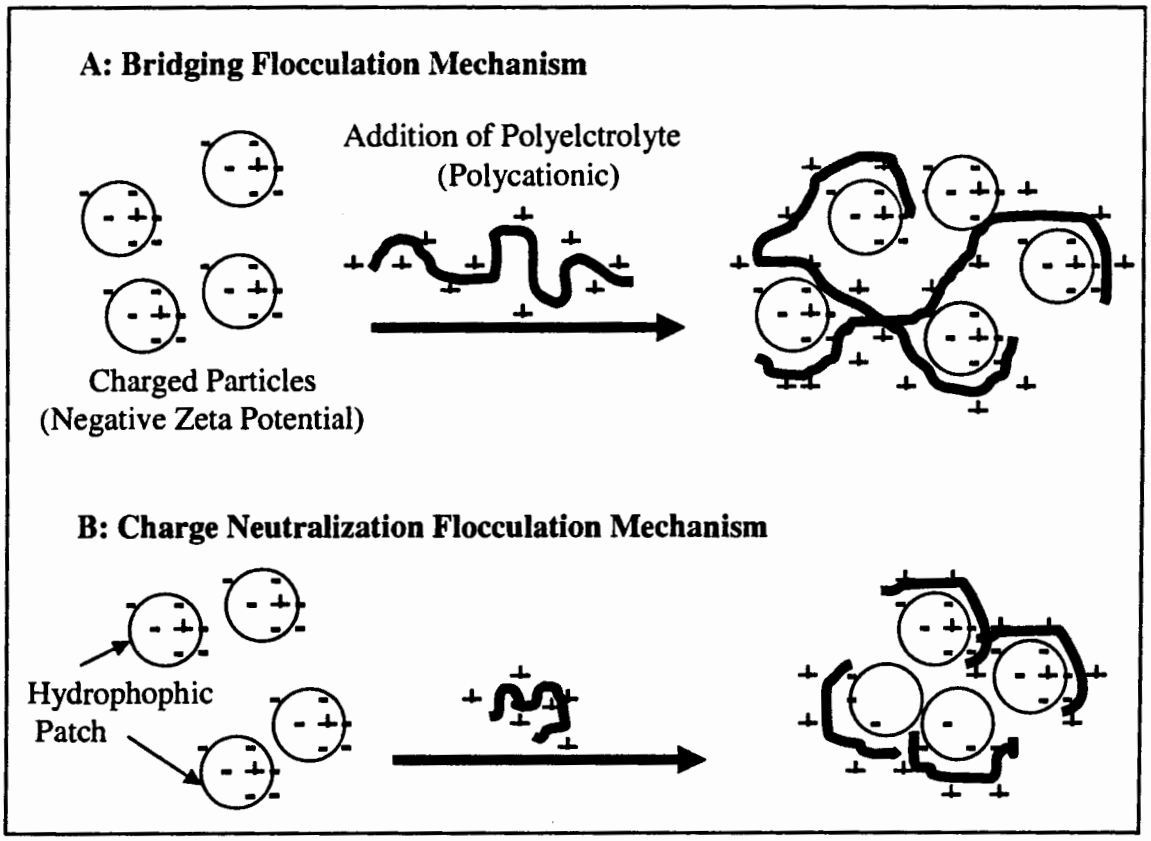

Figure 2: Representation of different mechanisms during flocculation of suspended solids with polyelectrolytes.

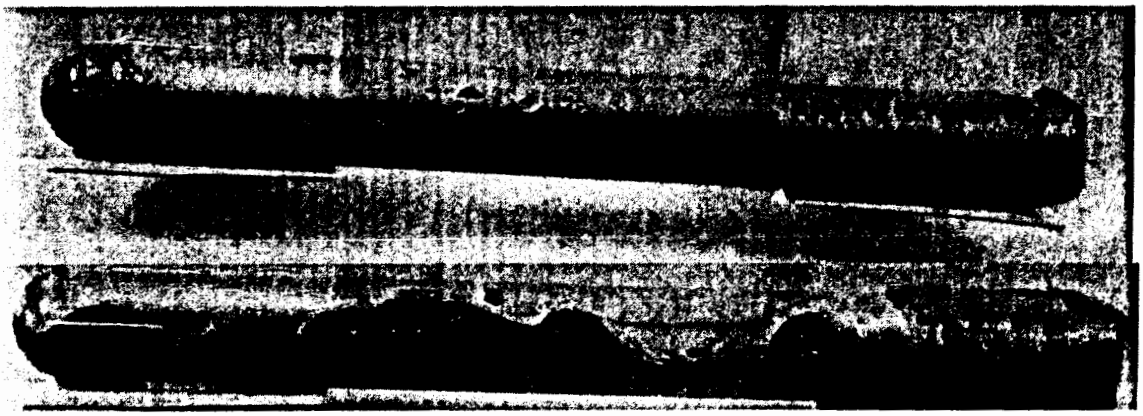

Figure 3: Flocculation of Ponderosa Pine hydrolyzate before (top) and after (bottom) addition of 1000 mg/L of Kemira C1592 polyelectrolyte.

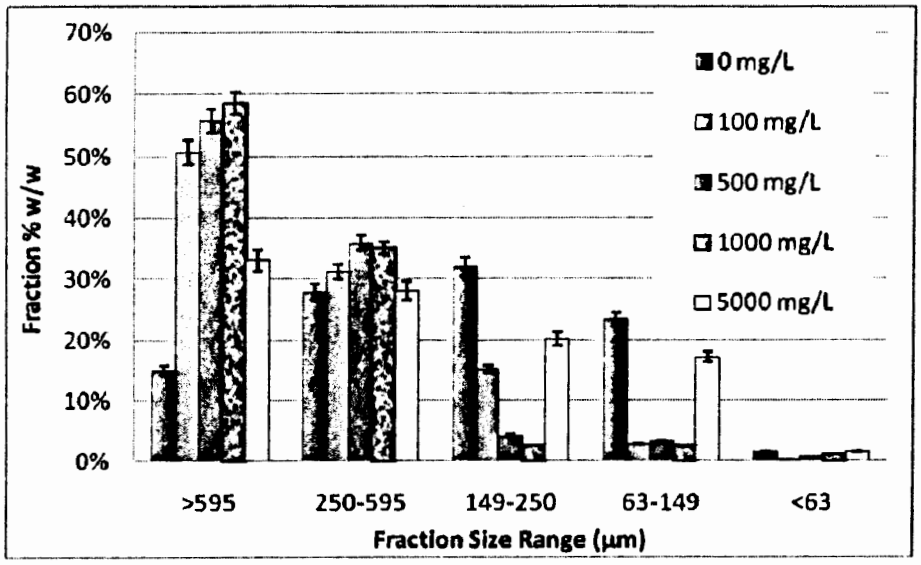

Figure 4: Particle size distribution of suspended solids in flocculated and non-flocculated ponderosa pine hydrolyzate. Error bars represent the range of two samples.

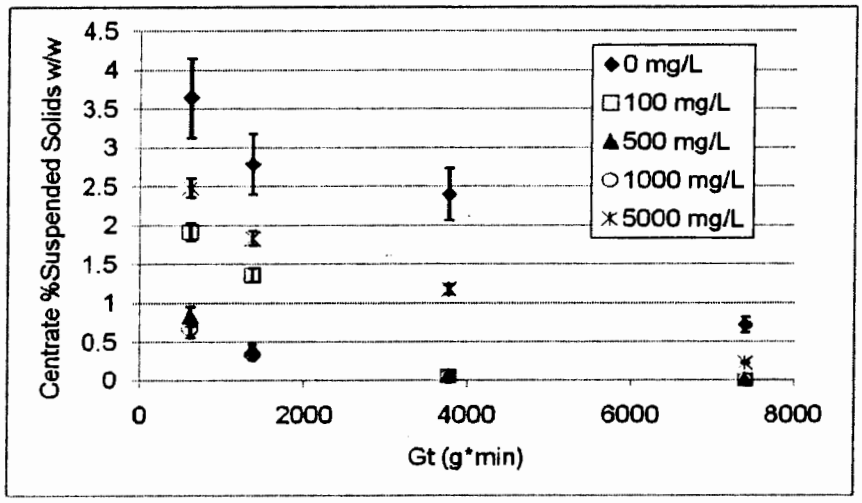

Figure 5: Percentage of suspended solids in the clarified centrate following flocculation of ponderosa pine hydrolyzate with C1592 polymer. Error bars represent the standard deviation of 3 samples.

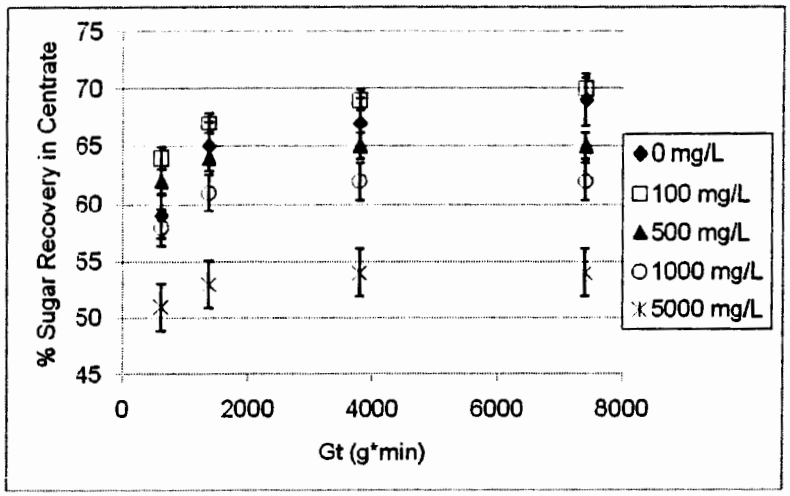

Figure 6: Percentage sugars recovery in the clarified centrate following flocculation of ponderosa pine hydrolyzate with C1592 polymer. Error bars represent the standard deviation of 3 samples.

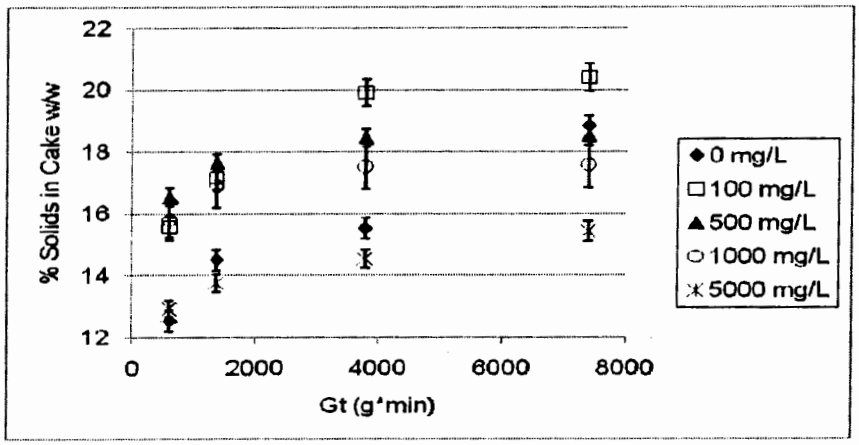

Figure 7: Percentage solids in the recovery solids cake following flocculation of ponderosa pine hydrolyzate with C1592 polymer. Error bars represent the standard deviation of 3 samples.

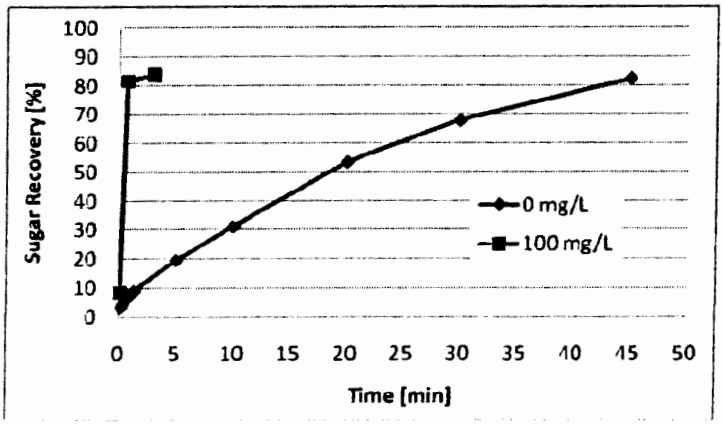

Figure 8: Cumulative sugar recovery during filtration of flocculated and unfloccualted pine hydrolyzate.

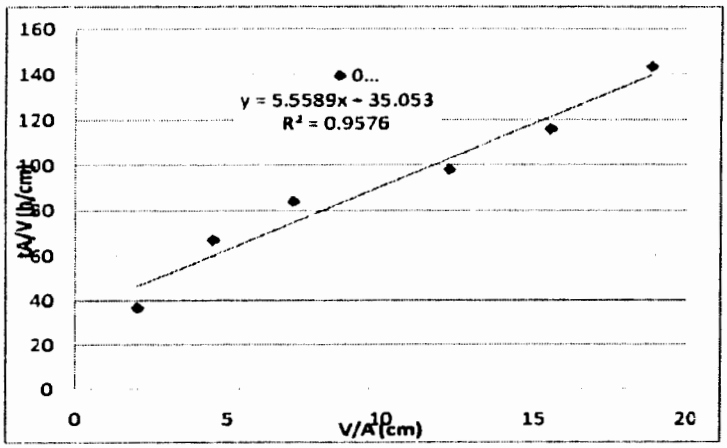

Figure 9: Filtration Darcy's Law plot for determination of membrane resistance and cake resistance during filtration of unflocculated pine hydrolyzate.

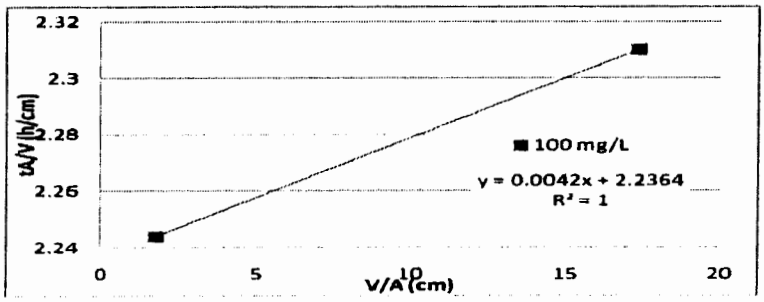

Figure 10: Filtration Darcy's Law plot for determination of membrane resistance and cake resistance during filtration of pine hydrolyzate after flocculation with 100 mg/L C1592 polymer.

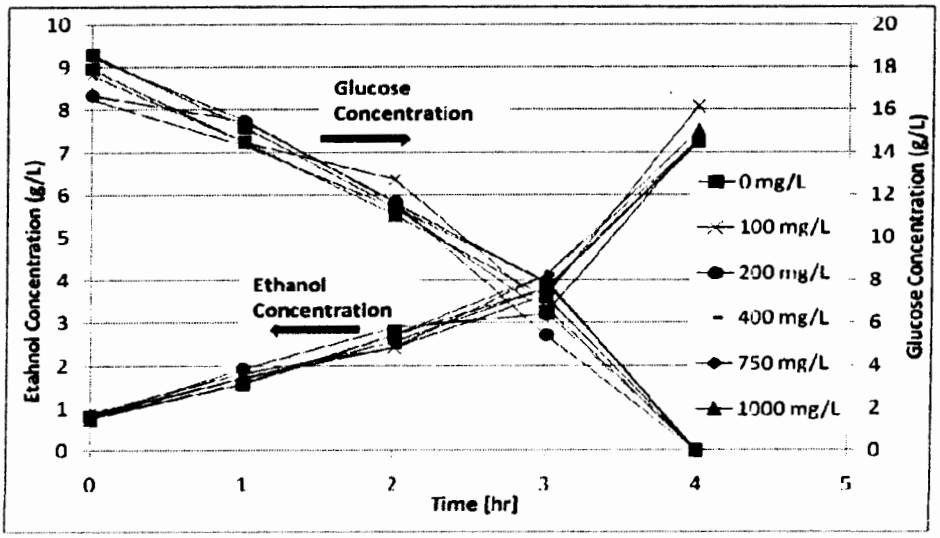

Figure 11: Ethanol fermentation with YPD media containing C1592 polyelectrolyte. Upward trending samples represent ethanol concentrations (left axis) and downward trending data represent glucose concentrations (right axis).

Removal and Recovery of Inhibitory Compounds from Pine Slurry Hydrolysates using a Polyelectrolyte Flocculating Agent

Brian Carter, Todd J. Menkhaus, and Patrick C. Gilcrease
Department of Chemical and Biological Engineering
South Dakota School of Mines and Technology
Rapid City, SD 57701

Abstract

Furfural, 5-hydroxymethylfurfural, and acetic acid are formed during the high temperature acidic pretreatment of cellulosic biomass (10); such pretreatments are used to increase the yield of fermentable sugars for the production of ethanol or other biorenewable products. These compounds inhibit ethanol fermentation by *Saccharomyces cerevisiae* at relatively low concentrations (e.g. furfural $\geq$ 1 g/L). Effective removal of these inhibitory compounds would allow the use of more severe pretreatment methods to improve sugar yields, leading to more efficient fermentations; if recovered and purified, these inhibitors could also be sold as valuable by-products. This study investigated the separation of inhibitory compounds from fermentable sugars by using polyethyleneimene (PEI), a soluble cationic polyelectrolyte flocculant. Due to the secondary amine structure of PEI, it participates in the Mannich reaction with aldehydes such as furfural and hydroxymethylfurfural. Experiments were performed on simple solutions and Pine slurry hydrolysates. The removal of inhibitory compounds from actual hydrolysates was evaluated as a function of wood particulate loading and enzyme concentration. Simple acetate solutions were evaluated as a function of sulfate concentration and solution pH. PEI added to simple solutions at a ratio of one mole of imine functional group to one mole inhibitor, removed up to 8.7, 59.0, and 64.5 wt% of acetic acid, 5-hydroxymethylfurfural, and furfural, respectively. The inclusion of wood particulates, or low pH conditions decreased the furfural and HMF removal. Furfural and 5-hydroxymethylfurfural were recovered after removal by washing the flocculant with an acid solution. Recoveries up to 81.0 and 97.0 wt% were achieved for furfural and 5-hydroxymethylfurfural, respectively. Results have shown that by choosing the appropriate conditions (pH 5, solids removed), the inhibitory aldehydes can be selectively removed with minimal (<3 wt. % glucose loss) fermentable sugar losses. The selective removal of inhibitory compounds may improve ethanol productivity and the specific growth rate of *Saccharomyces cerevisiae,* and may also provide a means to recover valuable coproducts.

Introduction

The world's continually increasing demands for energy and the limited supply of energy derived from fossil fuels have led to an increasing interest in alternative sources of energy (1, 4, 11). In recent years, ethanol fermentation from biomass feedstocks has gained attention. Sustainability, local availability, and low substrate cost are some of the advantages of using biomass (7). Another advantage is that fuel derived from biomass is not in direct competition with food production, as is the case with fuel derived from corn. Although ethanol production from biomass has been greatly improved, there are still areas that need further investigation including pretreatment, hydrolysis, solid-liquid clarification, and fermentation for the wide variety of feedstocks.

Overview of Cellulosic Ethanol Process

There are five major unit operations involved in the process of converting biomass to ethanol: pretreatment, enzymatic hydrolysis, solid-liquid separation, fermentation, and distillation (Figure 1).

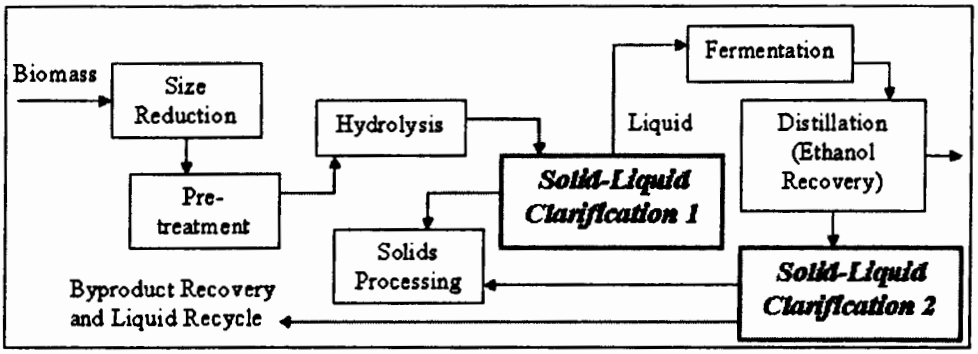

Figure 1: Process flow diagram depicting separate hydrolysis and fermentation

Pretreatment is required to alter the size, structure, and chemical composition so that enzymatic hydrolysis can be achieved more rapidly and with greater yields (8). There are several methods of pretreatment; however, dilute acid pretreatment has received considerable attention and was used in this research (6, 9). The addition of sulfuric acid to biomass results in the partial breakdown of cellulose to glucose and the hydrolysis of hemicellulose to xylose and other sugars (7). Glucose and xylose can further react to form 5-hydroxymethyl furfural (HMF) and furfural, respectively, in the presence of sulfuric acid at the high temperatures (160-220 °C) used during pretreatment (8). Furfural (Figure 2) and HMF (Figure 3) are both aldehydes and are inhibitory to microbial fermentation. The removal of these compounds will be important to produce a higher rate and yield of ethanol during fermentation.

The hydrolysis step uses cellulase enzymes to break down the cellulose chains into glucose. This is a required step to achieve the higher sugar yields needed for subsequent fermentations. Enzymatic hydrolysis operates at relatively mild conditions (50 °C and pH 5) for optimal cellulase activity. The cost of enzymes is a major factor in the economic feasibility of producing ethanol from biomass.

During the fermentation step, sugars formed in the pretreatment and hydrolysis steps are converted into ethanol. *Saccharomyces cerevisiae* is one of the most commonly used fermenting organisms due to its high ethanol yield and high ethanol tolerance; however, furfural and HMF inhibit ethanol production at concentrations as low as 1 g/L (5). Detoxification of the pretreated feed stock is necessary to achieve reasonable fermentation of the soluble sugars to ethanol.

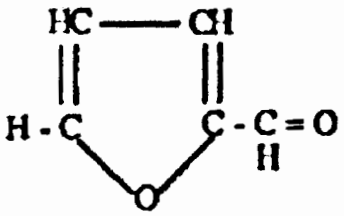

Figure 2: Furfural

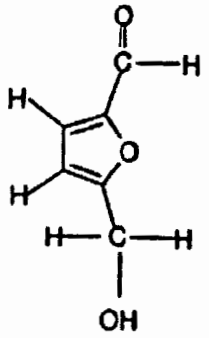

Figure 3: 5-Hydroxymethylfurfural

Flocculants

Flocculants are high molecular weight soluble chemicals that are traditionally used to promote the adsorption/aggregation of suspended solids, which can then settle out of solution or be separated by centrifugation or filtration. They can be polycationic, polyanionic, or nonionic. Polyethyleneimene (PEI), with a 60,000 molecular weight, was used in this research due to its secondary amine structure ($-CH_2-CH_2-NH_2^+-$). It was hypothesized that when PEI is mixed with a pine slurry hydrolyzate, it will undergo the Mannich reaction with the aldehydes furfural and HMF to form a Mannich base. The Mannich base polymer can then be removed by filtration with a molecular weight cut off (MWCO) membrane. This would produce a purified sugar solution for the fermentation step, resulting in a higher rate of ethanol production than if furfural and HMF were present. Recovery of furfural and HMF was also attempted by reversing the Mannich reaction; the Mannich base collected on the filter was washed with an acidic solution.

Materials and Methods

Pretreatment conditions

A 10 wt % Ponderosa pine slurry (4 L working volume) in a 1 wt% sulfuric acid solution was pretreated in a Parr reactor. The slurry was pretreated at 160-175 °C and 120-150 psig for 30 minutes. The Ponderosa pine sawdust was obtained from Baker Timber, Rapid City, SD and was sieved to a particle size below 800 microns. The pretreatment was performed to generate a complex mixture of sugars, inhibitory compounds, and wood solids. After removal from the Parr reactor, the slurry pH was adjusted to 5.0 with ammonium hydroxide. The final concentration ranges were 1.3-1.7 g/L for furfural and 0.6-0.8 g/L for HMF.

Enzymatic Hydrolysis

After pretreatment, the ponderosa pine slurry was enzymatically hydrolyzed in a 2 L Biostat B fermentor for 72 hrs at 50 °C and pH 5. Novozymes NS50013 (mixed cellulases) was added to the slurry at 30 FPU/g cellulose based on a stock concentration of 70 FPU/mL. Novozymes NS50010 (β-glucosidase) was added in a 1:10 volumetric ratio to NS50013. After 72 hours, the slurry was placed in a glass container and refrigerated at 4 °C to stop the enzymatic reaction.

Sample analysis

After PEI addition, liquid samples were vortexed for 3 seconds and centrifuged through a Centricon YM-10 10,000 molecular weight cut-off spin membrane on a VWR Clinical 100

centrifuge at 5800 RPM for 30 minutes to remove polyelectrolyte flocculants bound with inhibitory compounds. The filtrate was then measured for glucose, xylose, acetic acid, hydroxymethylfurfural, and furfural using a BioRad Aminex HPX-87H Ion Exclusion column on a Beckman Coulter HPLC with a System Gold Model 508 Autosampler, System Gold Model 125 Solvent Module, Timberline Instruments Model 105 Column Heater, and a Jasco RI-1530 Intelligent RI detector. The mobile phase (5 mM H_2SO_4) flowrate was set at 0.6 mL/min at a column temperature of 65 °C. Concentrations were determined from a calibration curve made from chemicals obtained from Fisher Scientific with a purity >99%.

Results and Discussion

Acetic Acid removal with PEI polymer (simple solution)

When PEI was added at a 1:1 molar ratio (PEI cation groups:acetate anion) to a 5 g/L acetic acid solution at a pH of 3.4, 89.1 wt% of the acetic acid was removed after ultrafiltration. When the pH of the acetic acid solution was adjusted to 7.0 with NaOH, no appreciable acetic acid was removed with the addition of PEI. Since PEI is basic (pH 11.2), it undergoes an acid/base neutralization reaction with acetic acid. At a solution pH of 3.4, this neutralization reaction occurs and acetic acid is removed. At a solution pH of 7.0, acetic acid has already reacted with NaOH and the OH^- competes with acetate for any PEI cation sites.

When sodium sulfate was added to the acetic acid solution, the sulfate ions compete with acetate for the cationic PEI binding sites. Sulfate ions will be present in a Ponderosa pine slurry because sulfuric acid is commonly used during dilute acid pretreatment. Figure 4 shows an 85% decrease in the removal of acetic acid as the amount of sodium sulfate was increased from 0 to 4.0 N.

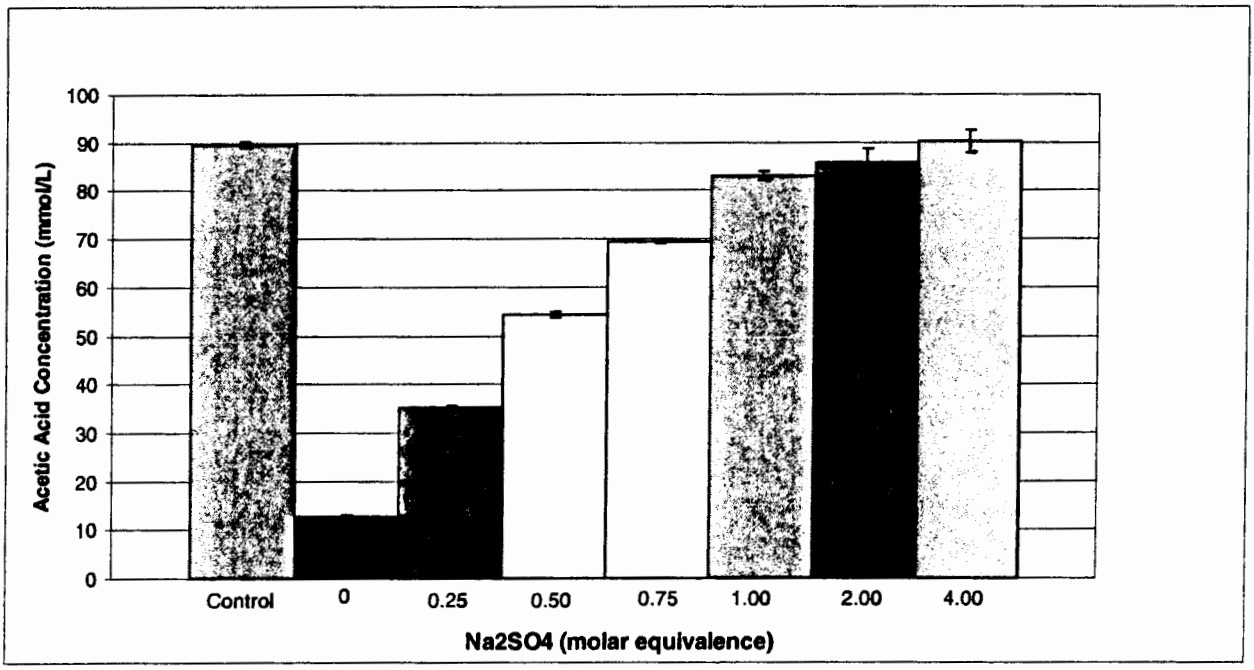

Figure 4: Effect of varying doses of Na_2SO_4 on acetic acid removal with PEI at pH 3.3. Control contained no sodium sulfate or PEI. (molar equivalents is ratio of PEI charge to $SO4^{2-}$ charge)

Effect of PEI on Glucose, Xylose, Furfural, and HMF removal (simple solutions)

An ideal separation would remove inhibitors from a lignocellulosic hydrolysate while retaining fermentable sugars in solution. From the results shown in Figure 5, glucose remains in solution following PEI addition and subsequent ultrafiltration, even at PEI molar equivalent dosages of 1:1. Xylose (not shown) behaved similarly to glucose and also remained in solution.

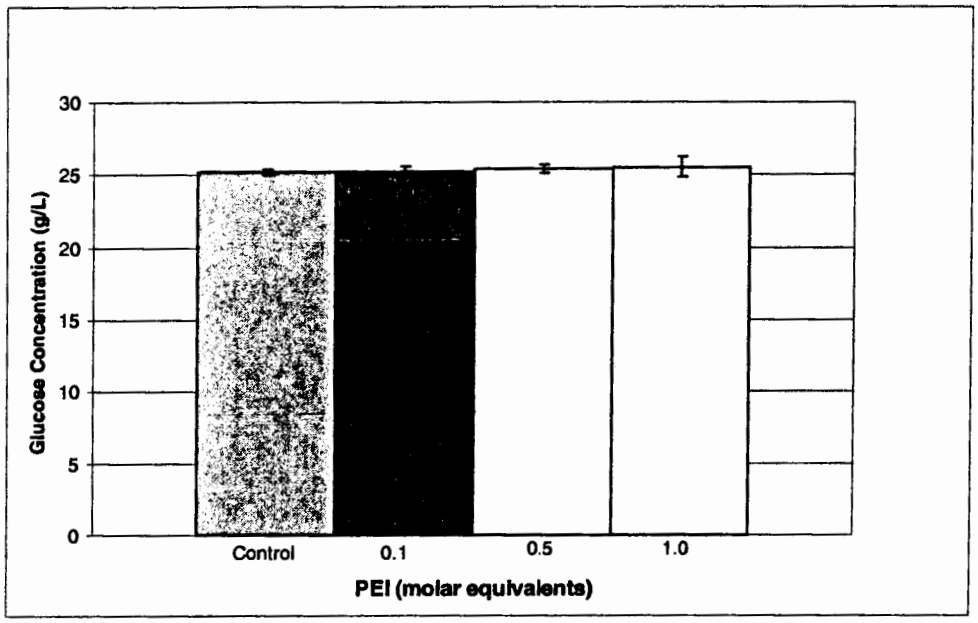

Figure 5: Effect of varying doses of PEI on glucose removal at pH 6.66

Figure 6 shows the results for the addition of PEI to a 2 g/L solution of furfural at a pH of 4.25. At a PEI to furfural molar equivalent ratio of 1:1, 81.5 wt% of the furfural was removed. When a 1:1 molar equivalent ratio of PEI was added to a 3 g/L solution of HMF (not shown) at a pH of 5.33, 58.6 wt% of the HMF was removed. The results shown here support the hypothesis that there is a covalent bonding mechanism (Mannich reaction) which allows for the removal of furfural and HMF via ultrafiltration of the PEI polymer.

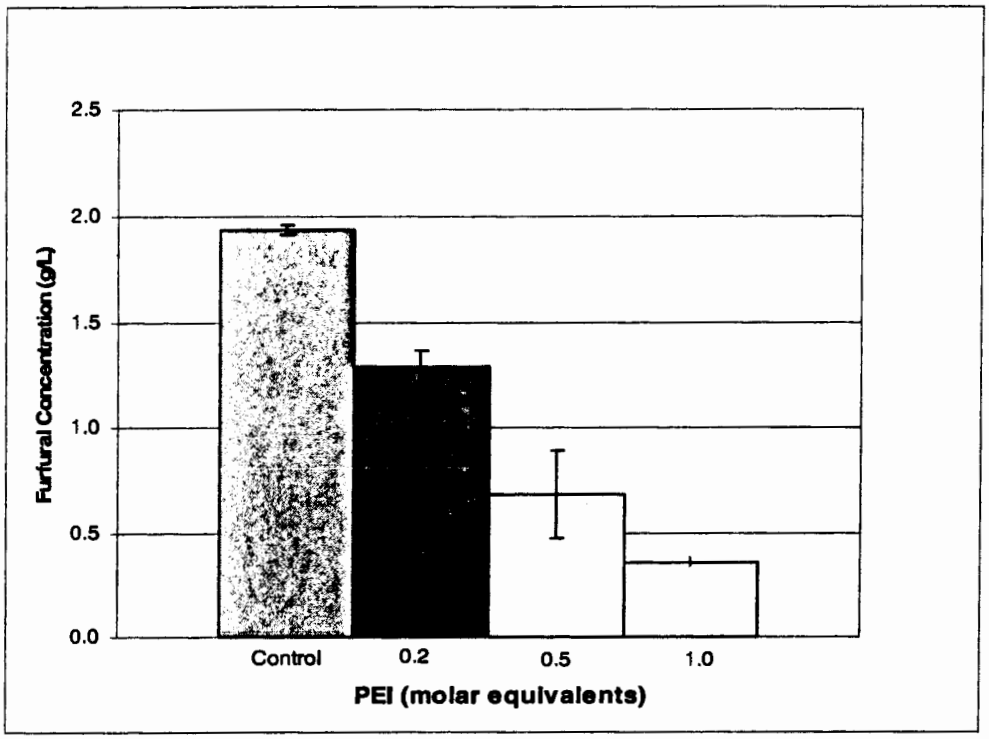

Figure 6: Effect of varying doses of PEI on furfural removal. PEI concentration at 1.0 molar equivalent equals 2.5 g/L

Effect of Enzymatic Hydrolysis on Furfural and HMF Removal from wood hydrolysates

The results for the simple solutions were promising; however, selective removal of furfural and HMF from a complex hydrolysate containing sugars, inhibitors, wood solids, and enzymes is needed. To test this, a PEI treatment was performed on a Ponderosa pine slurry before (pre-hydrolysis) and after (post-hydrolysis) it had undergone enzymatic hydrolysis. Prior to the addition of PEI, wood solids were removed with a 0.2 micron syringe filter. Glucose, xylose, acetic acid, furfural and HMF concentrations were quantified before and after the PEI treatment.

Since sulfuric acid was used in the pretreatment step, there were sulfate ions in solution, at a concentration of 204 mmol of (-) charge/L (4:1 ratio of sulfate (-) charge:acetate ion), which compete with the acetate ion for PEI cation sites. This prevented acetic acid from being removed from the slurry in both instances (6.84 wt% removal prehydrolysis and 0 wt% removal post-hydrolysis). After PEI addition and ultrafiltration, the concentrations of both glucose and xylose remained the same for both the pre and post-hydrolysis slurries. The level of furfural removed with PEI was reduced from 83.9 wt% removal for pre-hydrolysis to 24.1% removal for post-hydrolysis (Figures 7 and 8). The corresponding HMF removal percentage was also reduced from 66.4 wt% for pre-hydrolysis to 13.4 wt% post-hydrolysis (results not shown). Poor removal post-hydrolysis could be due to the enzymes present, the additional glucose being formed, or the increased surface area of lignin (exposed during cellulose digestion) competing with furfural and/or HMF for the PEI.

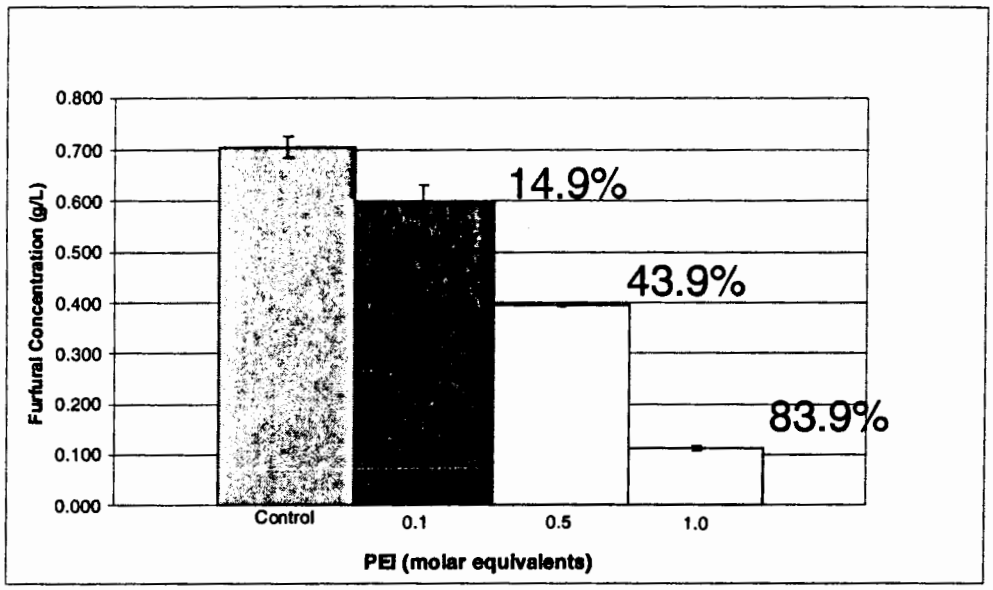

Figure 7: Furfural removal with PEI pre-hydrolysis (percentages shown are wt% removal)

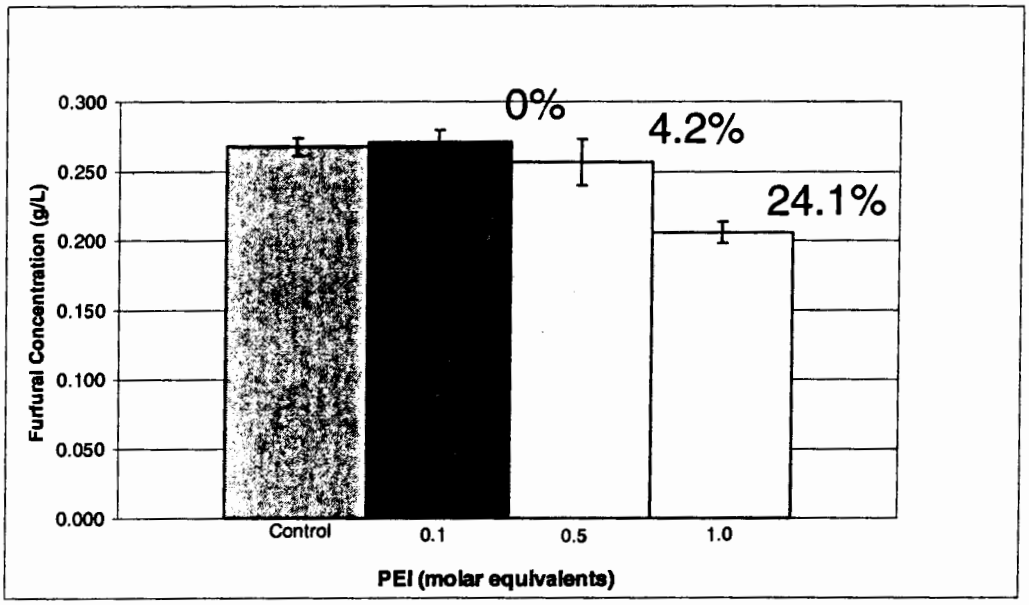

Figure 8: Furfural removal with PEI post-hydrolysis (percentages shown are wt% removal)

Effect of solids and/or enzymes on Furfural and HMF removal

To determine whether wood solids and/or enzymes have an effect on furfural and HMF removal post-hydrolysis, the fine solids were removed from the hydrolysate with a 10 kDa ultrafiltration membrane prior to PEI addition. The values in Fig. 9 are for the post-hydrolysis slurry (not filtered prior to PEI addition), while Fig. 10 shows furfural concentrations when the solids and enzymes were filtered out prior to PEI treatment. The furfural removal improved from 3.4 wt% to 29.1 wt% (1 molar equivalent of PEI) when the solution was filtered before PEI treatment. HMF removal improved from 1.5 wt% to 17.5 wt% at a 1 molar equivalent of PEI.

Since no sugars were removed with ultrafiltration, this indicates that either the enzymes or fine solid particles are competing with furfural and HMF for the PEI binding sites.

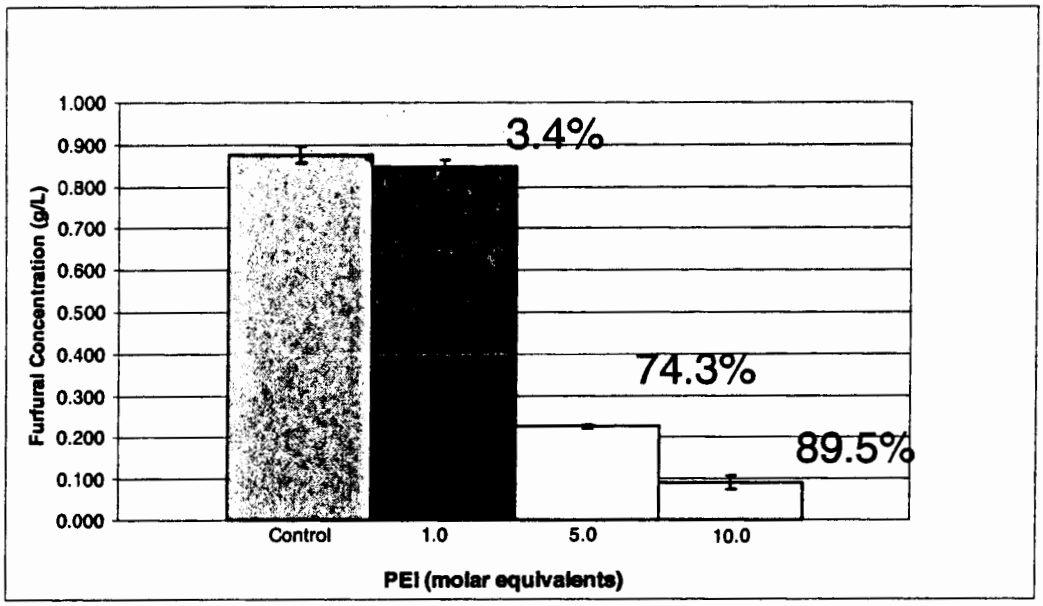

Figure 9: Furfural removal with PEI Post-hydrolysis, solids still present (percentages shown are wt% removal)

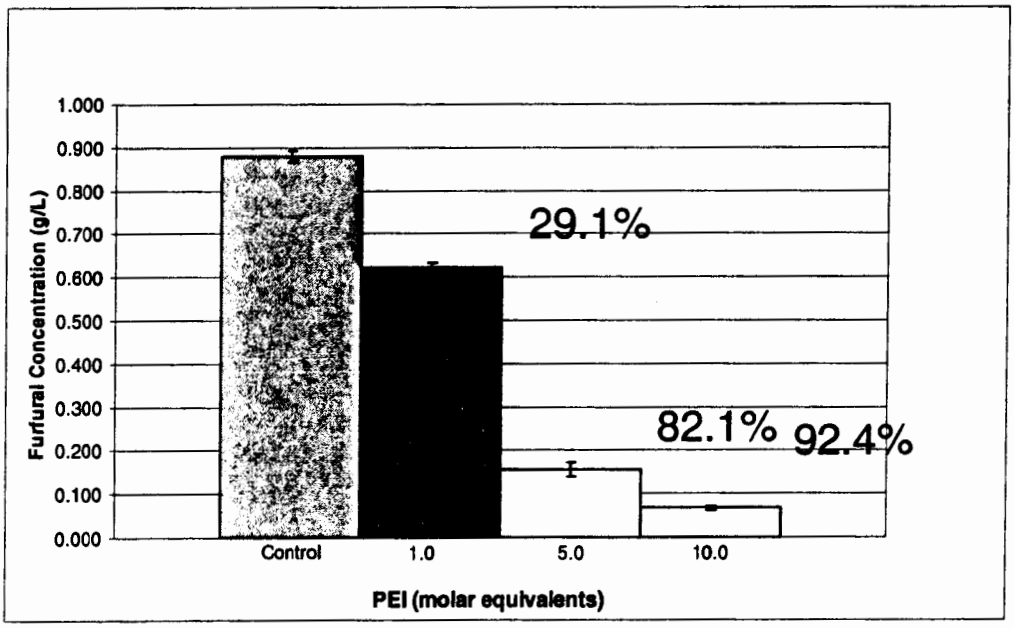

Figure 10: Furfural removal with PEI – post hydrolysis, solids filtered (10 kDa MWCO) prior to PEI treatment (percentages shown are wt% removal)

Effect of Enzymes on Furfural Removal

To determine whether cellulases have an effect on furfural and HMF removal with PEI, a simple 3.0 g/L solution of furfural was prepared which had a pH of 4.65. Novozymes Enzymes

NS50013 and NS50010 were added at a 30 FPU/g cellulose representation (as if the solution was produced from a 10 wt% wood slurry). Figure 11 shows the percent removal of furfural at 1.0 molar equivalent of PEI was very similar between the simple solution and the simple solution with enzymes present. This indicates that it was not the enzymes but the wood particulates that were competing with furfural for the PEI cation sites.

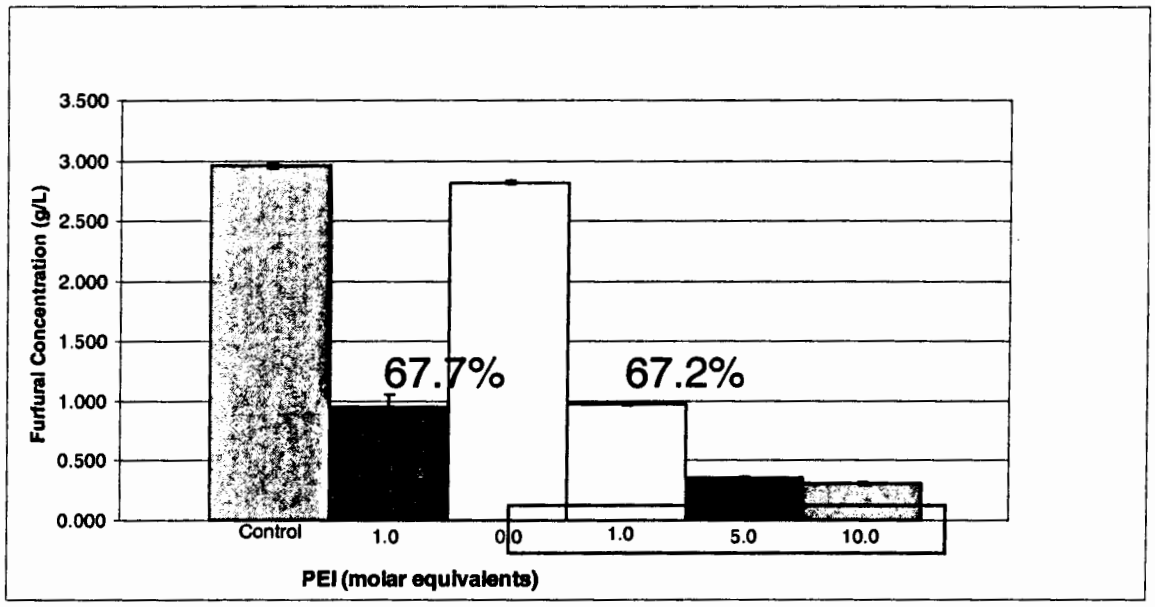

Figure 11: Effect of enzymes on Furfural removal with PEI; control was filtered through 10kDa membrane and contained no PEI or enzymes. Enzymes present at 30 FPU/g cellulose in last 4 experiments.

Furfural and 5-Hydroxymethylfurfural Recovery

The purpose of this experiment was to determine if furfural and HMF could be recovered after removal from solution with PEI. Based on the Mannich reaction mechanism, it was believed that the reaction could be reversed by decreasing the pH of the solution or by using a low pH acid wash (2). For this experiment, simple 3.0 g/L furfural and 3.0 g/L HMF solutions were prepared which had a pH of 4.22, and 4.45 respectively. PEI was added to each at a 1 molar equivalent amount and filtered with a 10 kDa MWCO spin membrane. A 1 mL sulfuric acid wash (various concentrations) was then added to the PEI-inhibitor complex, which remained on top of the filter. This mixture was vortexed and centrifuged to reverse the Mannich reaction and wash the furfural or HMF through the filter. The figures below show that 64.5% and 59.0% of furfural and HMF (results not shown), respectively, were removed in the first step. A sulfuric acid wash with pH 1.97 and 2.0 recovered 81.0 wt % and 96.9 wt % of the furfural and HMF, respectively, that was removed from solution in the first step.

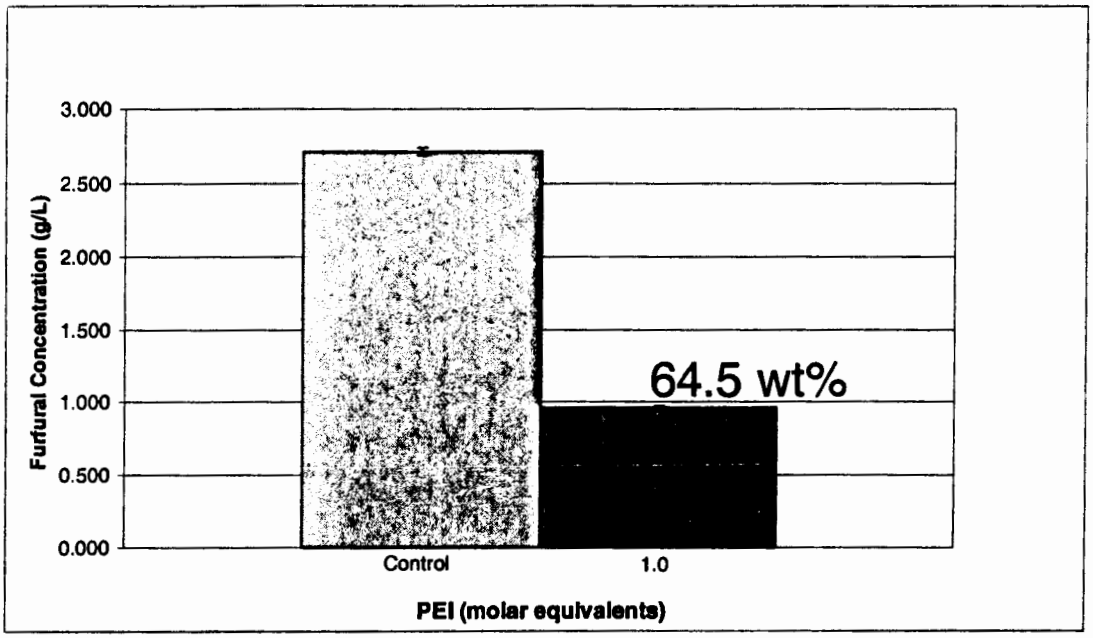

Figure 12: Furfural removal with PEI

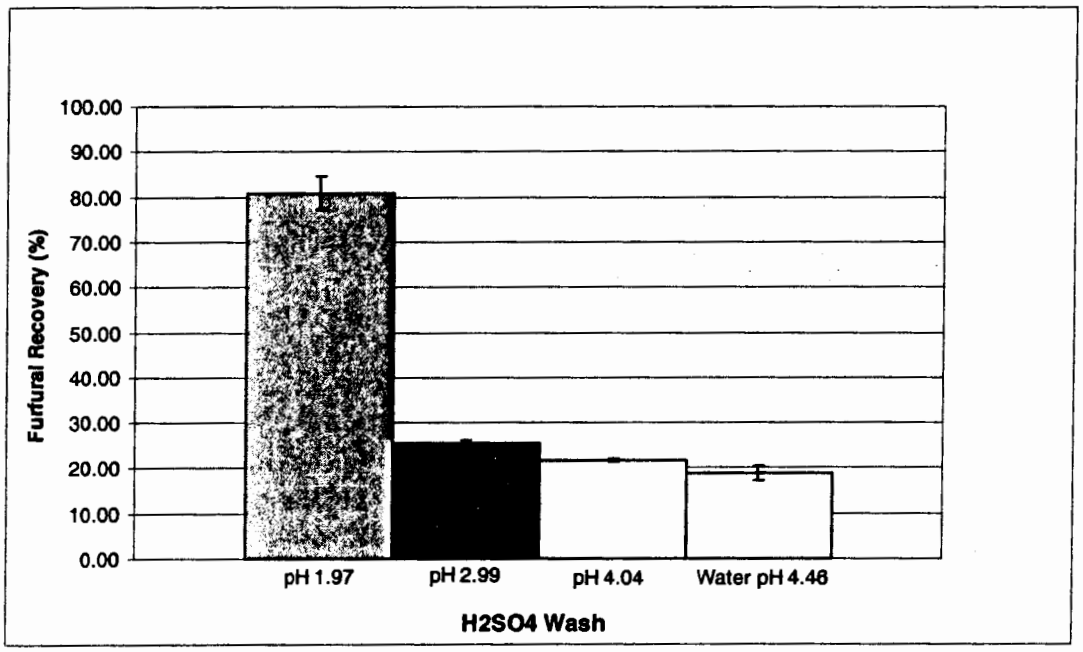

Figure 13: Furfural Recovery with sulfuric acid wash

Conclusion

Results have shown that by choosing the appropriate conditions (pH 5, fine particulates removed), the inhibition compounds furfural and HMF can be selectively removed with minimal (<3 wt. % glucose loss) fermentable sugar losses. Removal of acetic acid from pine hydrolysate slurries was insufficient, (presumably due to the interaction of other ions with the polyethyleneimene flocculant) and may need to be removed using other separation methods. If fine wood particles are present, an increase in flocculant dose may be needed due to the

interaction of the negative surface charge of the wood and the positive charge of the amine groups on the flocculant. The selective removal of inhibitory compounds may improve ethanol productivity and the specific growth rate of *Saccharomyces cerevisiae* when the hydrolysate is fermented, and may also provide a means to recover these aldehydes as valuable coproducts.

References

1. Aristidou A., M. Penttila. Metabolic engineering applications to renewable resource utilization. *Current Opinions in Biotechnology*. 2000; 11, 187-198.
2. Blackburn, T.B. The Mannich reaction. Mechanistic and technological considerations. *Journal of Pharmaceutical Sciences*. 1968; 57, 715-733.
3. Jacobsen, S.E., C.E. Wyman. Hemicellulose and cellulose hydrolysis models for application to current and novel pretreatment processes. *Applied Biochemistry and Biotechnology*. 1999; 81-96.
4. Jeffries, T.W., Y.S. Jin. Ethanol and thermotolerance in the bioconversion of xylose by yeasts. *Adv Appl Microbiol*. 2000; 47, 221-268
5. Klinke, H. B., A. B. Thomsen, B. K. Ahring. Inhibition of ethanol-producing yeast and bacteria by degradation products produced during pre-treatment of biomass. *Applied Microbiology and Biotechnology*. 2004; 66, 10-26.
6. Lee, Y.Y., P. Iyer, R.W. Torget. Dilute-acid hydrolysis of lignocellulosic biomass. *Advances in Biochemical Engineering and Biotechnology*. 1999; 65, 93.
7. Lin, Y., S. Tanaka. Ethanol fermentation from biomass resources: current state and prospects. *Applied Microbiology and Biotechnology*. 2006; 69, 627-642.
8. Mosier, N., C. Wyman, B. Dale, R. Elander, Y. Y. Lee, M. Holtzapple, M. Ladisch. Features of promising technologies for pretreatment of lignocellulosic biomass. *Bioresource Technology*. 2005; 96, 673-686.
9. Tsao, G. T., M. Ladisch, M. Voloch, P. Bienkowski. Production of ethanol and chemicals from cellulosic materials. *Process Biochemistry*. 1982; 17, 34-38.
10. Weil, J. R., B. Dien, R. Bothast, R. Hendrickson, N. S. Mosier, M. Ladisch. Removal of Fermentation Inhibitors Formed during Pretreatment of Biomass by Polymeric Adsorbents. *Ind. Eng. Chem. Res*. 2002; 41, 6132-6138.
11. Zaldivar J., J. Nielsen, L. Olsson. Fuel ethanol production from lignocellulose: a challenge for metabolic engineering and process integration. *Appl Microbiol Biotechnol*. 2001; 56, 17-34.

The thioesterases: A new perspective based on their primary and tertiary structures

David C. Cantu, Yingfei Chen, and Peter J. Reilly
Department of Chemical and Biological Engineering, Iowa State University, Ames, IA 50011

The thioesterases have been classified into EC 3.1.2.1 through EC 3.1.2.27 based on their activities on different substrates, with many remaining unclassified (EC 3.1.2.–). Analysis of thioesterases with known primary and tertiary structures contained in the new ThYme (Thioester-active enzYmes) database casts a new light on this enzyme group. At present, the thioesterases fall into 32 families unrelated by amino acid sequence. These families encompass 14 EC numbers linked to thioesterases, with the other 13 EC numbers not being represented by primary structures in various queried databases. Several thioesterases with single EC numbers (acetyl-CoA hydrolase, EC 3.1.2.1; palmitoyl-CoA hydrolase, EC 3.1.2.2; oleoyl-ACP hydrolase, EC 3.1.2.14; and ubiquitin thiolesterase, EC 3.1.2.15) are found in more than one family. It is assumed that all members of the same family have essentially the same tertiary structure; however, thioesterases in different families can have markedly different folds. Furthermore, it is possible for members of different families to have very similar tertiary structures despite not being related by primary structure, indicating that they have common distant ancestors and can be grouped into clans.

Introduction

The thioesterases (TEs), or thioester hydrolases, comprise a large enzyme group whose members hydrolyze the thioester bond between a carbonyl group and a sulfur atom. They are classified into EC (Enzyme Commission) 3.1.2.1 to EC 3.1.2.27, as well as EC 3.1.2.– for unclassified TEs (NC-IUBMB, 1992). Substrates of 15 of these 27 groupings contain coenzyme A (CoA), two contain acyl carrier proteins (ACPs), four have glutathione or its derivatives, one possesses ubiquitin, and two contain other moieties. In addition, three groupings have been deleted.

The EC classification is based on enzyme function and substrate identity, and it was formulated when very few amino acid sequences (primary structures) and three-dimensional (tertiary) structures of enzymes were available. Another way to classify enzymes is by structure, and many databases such as CAZy for carbohydrate-active enzymes (Cantarel *et al.*, 2009) have done this. It is common to observe that members of more than one EC grouping are found in one enzyme family based on similar amino acid sequences, implying that they have a common ancestor, mechanism, and tertiary structure. Conversely, members of a single EC grouping may be located in more than one enzyme family, being unrelated in primary structure and potentially in mechanism and tertiary structure.

A further observation is that members of two different enzyme families may have very similar tertiary structures and mechanisms even though their primary structures are very different. This may imply that they are members of the same clan, descended from a more distant ancestor.

We have constructed a new database, ThYme (Thioester-active enzYmes, http://www.enzyme.cbirc.iastate.edu) that classifies several enzyme groups, including the TEs, into families based on similar primary structures. We have used it draw conclusions on how the TEs are divided (and united) by not only primary structure, but also by tertiary structure. This article is an account of that effort.

Construction of thioesterase families and clans

TE families were identified by using the Basic Local Alignment Search Tool (BLAST) (Altschul *et al.*, 1997) on the catalytic domains of query TE sequences. The uniqueness of the families was confirmed by multiple sequence alignments (MSA) and by their tertiary structures.

Query sequences were taken from EC 3.1.2.1 to EC 3.1.2.27 and EC 3.1.2.– entries in the UniProt database (UniProt Consortium, 2008). Only reviewed Swiss-Prot (Bairoch and Apweiler, 2000) entries, which have a higher level of annotation, and those noted by "Evidence at Protein Level", were used. Those described by "Inferred from Homology" or "Evidence at Transcript Level", as well as fragments and putative or probable enzymes, were excluded from the query sequences. The 206 sequences that met these criteria at that time made up the query sequence list. This list contained only 11 of the 27 TE EC numbers, as well as sequences having EC 3.1.2.– numbers, whereas 16 EC numbers did not meet these criteria, had no sequences, or had been deleted by the NC-IUBMB.

The first entry from the query sequence list was compared to the National Center for Biotechnology Information's (NCBI) GenBank (Benson *et al.*, 2009) nr peptide sequence database using BLAST. The protein–protein BLAST algorithm was used, the cutoff *E*-value was set to 0.001, and Max Target Sequences was set to 10,000 to ensure that all results with $E = 0.001$ or less were reported. All other parameters were default values. Later query sequences found in the BLAST results were deleted from the list. The remaining query sequences were subjected to BLAST in turn until all the listed sequences were either deleted or used. To automate this step, blast-2.2.19 was downloaded from NCBI's webpage (http://www.ncbi.nlm.nih.gov/staff/tao/URLAPI/unix_setup.html) and installed on a Unix platform. The nr peptide sequence database was also downloaded from this URL and updated before using BLAST. A script was written to successively use BLAST, compare results, and delete retrieved query sequence list members automatically.

After the first BLAST run, catalytic domains of the query sequences in each BLAST output file were identified from the Pfam database (Finn *et al.*, 2008) by searching the query sequence. Then the query sequences were modified to include only the catalytic domain and subjected to BLAST again. If Pfam did not identify a domain with TE activity, MSAs using ClustalX 2.0 (Larkin *et al.*, 2007) or MUSCLE 3.6 (Edgar, 2004) were performed on ~50 random sequences from the BLAST output file of the corresponding query sequence. Then profile hidden Markov models (Eddy, 1998) using hmmer-2.3.3 (http://hmmer.janelia.org) were used to identify a conserved domain in those sequences that was likely to be the catalytic domain. Also, the deleted query sequences from the original list were checked to ascertain whether they contained catalytic domains not included in the query sequences of the BLAST output files (not the case with TEs).

These procedures yielded BLAST output files making up each family. MSAs were then constructed to confirm or disallow each BLAST output file as a single family, or to check whether two or more output files should be merged into one family.

MSAs were constructed by randomly selecting ~50 sequences from one or more BLAST output files. If a sequence entry appeared in more than one BLAST output file, suggesting that these output files comprise one family, equal numbers of sequences were taken from each output files to obtain ~50 sequences in total. Then the FASTA format of these sequences were retrieved from Batch Entrez (http://www.ncbi.nlm.nih.gov/sites/batchentrez?db=Protein), and sequences of protein fragments were deleted. Clustal X and MUSCLE default parameters were used. Sufficient conservation of residues and residue chemical character confirms the presence of a single family. Lack of conservation suggests that more than one family exists, and if so, MSAs

were performed on smaller sets of sequences.

All tertiary structures from the BLAST output files were obtained from the Research Collaboratory for Structural Bioinformatics Protein Data Bank (RCSB PDB) webpage (www.rcsb.org) and compared within one family and among families. PyMOL version 1.1 (DeLano Scientific, Palo Alto, CA; http://www.pymol.org/) was used to select the monomer of each PDB file containing the TE catalytic domain. Those structures were then superimposed with MultiProt version 1.0 (Shatsky *et al.*, 2004). MultiProt scoring and biocore parameters were both set to 2, with all other parameters remaining at their default values. All the chains within one family were superimposed in MultiProt and their root mean square deviations (RMSDs) were recorded.

Once the families were defined and confirmed by MSA and tertiary structure conservation, MultiProt was used to superimpose tertiary structures of different families. Those families with similar tertiary structures are grouped into clans.

Results and Discussion

Thioesterase family classification

Use of BLAST with TE query sequences followed by construction of MSAs and superposition of tertiary structures yielded 32 families unrelated by primary structure (Table I). Among them, enzymes in 11 families (TE1–TE6, TE13, TE14, TE28, TE29, and TE32) are active on substrates containing various acyl moieties and CoA, TEs in two families (TE7 and TE8) break bonds between acyl groups and glutathione and its derivatives, those in four families (TE9–TE12) attack bonds between acyl groups and ACP, and those in 11 families (TE16–TE26) appear to break bonds between ubiquitin and different thiols. Members of TE27 cleave the bond between acyl groups and proteins. TE15, TE30, and TE31 members are overwhelmingly not TEs, with their occasional TEs having yet undefined functions. With CoA and ACP, the sulfur-carrying moiety is a pantethiene residue, while with various glutathiones and non-ACP proteins, the sulfur-carrying moiety is built up from a cysteine residue.

A number of families (TE6, TE8–TE10, TE13, TE15, TE20, TE21, TE29–TE31) have only a minority of TE members, even though TE query sequences were used to locate them. TE20 and TE21 are classified as TE families because ubiquitin thiolesterase query sequences isolated their members and because they were produced by eukaryota only, characteristic of ubiquitin thiolesterases and acyl-protein hydrolases.

These TE families bear rather limited resemblance to EC numbers representing TEs. For instance, acetyl-CoA hydrolases (3.1.2.1) occur in TE1 and TE2, palmitoyl-CoA hydrolases (EC 3.1.2.2) occur in TE2, TE4, and TE5, oleoyl-ACP hydrolases (EC 3.1.2.14) are found in TE9–TE12, and ubiquitin thiolesterases (EC 3.1.2.15) occur in TE15–TE26 (Table I). Conversely, of the 24 EC numbers remaining after three deletions, only 14 of them (EC 3.1.2.1, 3.1.2.2, 3.1.2.4, 3.1.2.6, 3.1.2.12, 3.1.2.14, 3.1.2.15, 3.2.1.18, 3.1.2.19, 3.1.2.20, 3.1.2.22, 3.1.2.23, 3.2.1.26, and 3.1.2.27) are found in significant numbers among the 32 TE families. Of course, further EC numbers characteristic of TEs will likely appear as more TEs are sequenced and characterized.

These results show the effects of both convergent and divergent evolution. The former is exemplified by the fact that members of nearly all the 32 families, most descended from different ancestors, are active on substrates that contain the thioester group, and most attack the bond between its carbonyl carbon atom and its adjacent sulfur atom. More specifically, four enzymes with four separate names and EC numbers are found in 19 different TE families. Divergent evolution is shown by the limited variation of primary, secondary, and tertiary structures within

the same TE family, and by the possibility of more profound variation of primary structure so that two or more families are members of the same clan, without primary structure conservation.

Thioesterase tertiary structures

Most TE families have at least one member with a known tertiary structure. Some examples are found in Figures 1–5. Figure 1 shows the superposition of two tertiary structures of TE1 members. Figure 2 has five superimposed TE2 structures, one of which has extra α-helices and β-strands giving a double hot dog fold. Figures 3–5 show TE9, TE12, and TE13 structures.

Funding

The authors are grateful for the support of the U. S. National Science Foundation through its Engineering Research Center Program (Award No. EEC-0813570), leading to the formation of the Center for Biorenewable Chemicals (CBiRC) at Iowa State University and a number of other universities and research centers.

Acknowledgements

The authors thank Luis Petersen for his initial help in writing the scripts to automate BLAST.

References

Altschul, S.F., Madden, T.L., Schäffer, A.A., Zhang, J., Zhang, Z., Miller, W., and Lipman, D.J. (1997) *Nucleic Acids Res.*, **25**, 3389–2402. http://blast.ncbi.nlm.nih.gov/Blast.cgi.

Bairoch, A., and Apweiler, R. (2000) *Nucleic Acids Res.*, **28**, 45–48.

Benson, D.A., Karsch-Mizrachi, I., Lipman, D.J., Ostell, J., and Sayers, E.W. (2009) *Nucleic Acids Res.*, **37**, D26–D31. http://www.ncbi.nlm.nih.gov/Genbank/.

Cantarel, B.L., Coutinho, P.M., Rancurel, C., Bernard, T., Lombard, V., and Henrissat, B. (2009) *Nucleic Acids Res.*, **37**, D233–2388. http://www.cazy.org.

Eddy, S.R. (1998) *Bioinformatics Rev.*, **14**, 755–763.

Edgar, R.C. (2004). *Nucleic Acids Res.* **32**, 1792–1797. http://www.drive5.com/muscle/.

Finn, R.D., Tate, J., Mistry, J., Coggill, P.C., Sammut, S.J., Hotz, H.R., Ceric, G., Forslund, C., Eddy, S.R., Sonnhammer, E.L.L., and Bateman, A. (2008) *Nucleic Acids Res.*, **36**, D281–D288. http://pfam.sanger.ac.uk/.

Larkin, M.A., Blackshields, G., Brown, N.P., Chenna, R., McGettigan, P.A., McWilliam, H., Valentin, F., Wallace, I.M., Wilm, A., Lopez, R., Thompson, J.D., Gibson, T.J., and Higgins, D.G. (2007) *Bioinformatics*, **23**, 2947–2948. http://www.clustal.org/.

Nomenclature Committee of the International Union of Biochemistry and Molecular Biology (NC-IUBMB) (1992). Enzyme Nomenclature. Academic Press, San Diego, CA. http://www.chem.qmul.ac.uk/iubmb/enzyme/.

Shatsky, M., Nussinov, R., and Wolfson, H.J. 2004. *Proteins Struct. Funct. Bioinformat.*. **56**, 143–156. http://bioinfo3d.cs.tau.ac.il/MultiProt/.

UniProt Consortium (2008) *Nucleic Acids Res.*, **36**, D190–D195. http://www.uniprot.org.

Table I. Thioesterase families classified by amino acid sequence similarity

Families	EC Numbers[1]	Enzymes[2]	Producing organisms
1	3.1.2.1	Acetyl-CoA hydrolases	Bacteria, eukaryota, archaea
	2.8.3.–	Unclassified CoA transferases	
2	3.1.2.–	Unclassified thioesterases[3]	Bacteria, eukaryota, archaea
	3.1.2.1	Acetyl-CoA hydrolases	
	3.1.2.2	Palmitoyl-CoA hydrolases	
	3.1.2.19	ADP-dependent medium-chain acyl-CoA hydrolases	
	3.1.2.20	Acyl-CoA hydrolases	
3	3.1.2.–	Unclassified thioesterases[3]	Bacteria
	3.1.2.18	ADP-dependent short-chain acyl-CoA hydrolases	
4	3.1.2.2	Palmitoyl-CoA hydrolases	Eukaryota, bacteria
5	3.1.2.2	Palmitoyl-CoA hydrolases	Bacteria, eukaryota
	3.1.2.27	Choloyl-CoA hydrolase	
6	4.2.1.17	Enoyl-CoA hydratases	Bacteria, eukaryota
	4.2.1.55	3-Hydroxybutyryl-CoA hydratases	
	3.1.2.4	3-Hydroxyisobutyryl-CoA hydrolases	
	5.1.2.3	3-Hydroxyisobutyryl-CoA epimerases	
	1.1.1.35	3-Hydroxyacyl-CoA dehydrogenases	
7	3.1.2.6	Hydroxyacylglutathione hydrolases	Bacteria, eukaryota
8	3.1.1.1	Carboxyesterases	Bacteria, eukaryota
	3.1.2.12	S-formylglutathione hydrolases	
9	2.3.1.–	Unclassified acyltransferases	Bacteria, eukaryota
	3.1.2.14	Oleoyl-ACP hydrolases (TE domains of fatty acid synthases, ketoacyl synthases, and polyketide synthases)	
10	2.3.1.38	ACP S-acetyltransferases	Bacteria, eukaryota
	2.3.1.85	Fatty-acid synthases	
	3.1.2.14	Oleoyl-ACP hydrolases (TE domains of fatty-acid synthases, ketoacyl synthases, and polyketide synthases)	
11	3.1.2.14	Oleoyl-ACP hydrolases	Bacteria, eukaryota
	3.1.2.–	Unclassified TEs	
12	3.1.2.14	Oleoyl-ACP hydrolases	Eukaryota, bacteria
13	3.1.1.2	Arylesterases	Bacteria
	3.1.2.–	Unclassified TEs[3]	
	3.1.1.5	Lysophospholipases	
14	3.1.2.–	Unclassified TEs[3]	Eukaryota, bacteria

15	3.1.1.1	Carboxylesterases/phospholipases	Bacteria, eukaryota
	3.1.2.–	Unclassified TEs[4]	
16	3.1.2.15	Ubiquitin thiolesterases	Eukaryota
17	3.1.2.15	Ubiquitin thiolesterases	Eukaryota
18	3.1.2.15	Ubiquitin thiolesterases	Eukaryota
19	3.1.2.–	Unclassified TEs[5]	Eukaryota
20	—	Hypothetical and predicted proteins	Eukaryota
	3.1.2.–	Unclassified TEs[5]	
21	3.1.2.–	Hypothetical and predicted proteins	Eukaryota
22	3.1.2.–	Unclassified TEs[5]	Eukaryota
23	3.4.19.12	Ubiquitin C-terminal hydrolases	Eukaryota
	3.1.2.15	Ubiquitin thiolesterases	
24	3.1.2.15	Ubiquitin thiolesterases	Eukaryota
25	3.1.2.15	Ubiquitin thiolesterases	Eukaryota
26	3.1.2.15	Ubiquitin thiolesterases	Eukaryota
27	3.1.2.22	Palmitoyl-protein hydrolases	Eukaryota
28	3.1.2.23	4-hydroxybenzoyl-CoA thioesterase	Bacteria
29	2.8.3.16	Formyl-CoA transferases	Bacteria, eukaryota, archaea
	5.1.99.4	α-Methylacyl-CoA racemases	
	3.1.2.26	Bile acid-CoA hydrolases	
30	—	Hypothetical and predicted proteins	Bacteria, eukaryota, archaea
	3.1.2.–	Unclassified TEs	
31	3.1.1.1	Carboxylesterases	Eukaryota, bacteria, archaea
	3.1.1.7	Acetylcholinesterases	
	3.1.2.–	Unclassified TEs	
32	3.1.1.11	Pectinesterases	Bacteria
	3.1.2.–	Unclassified TEs[3]	

[1] In order of most frequent listing.
[2] Official enzyme name associated with EC number.
[3] Acyl-CoA hydrolase frequently listed.
[4] Lysophospholipase and acyl-protein thioesterase frequently listed
[5] Ubiquitin thiolesterase frequently listed.

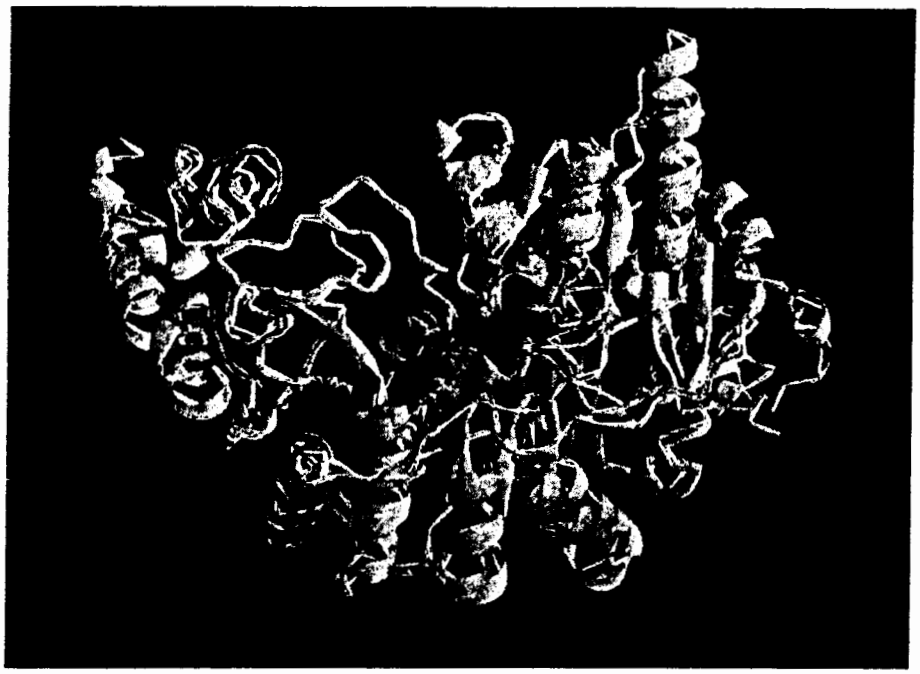

Figure 1. Two superimposed TE1 tertiary structures.

Figure 2. Five superimposed TE2 tertiary structures, with one having two extra α-helices and five extra β-strands, giving it a double hotdog fold.

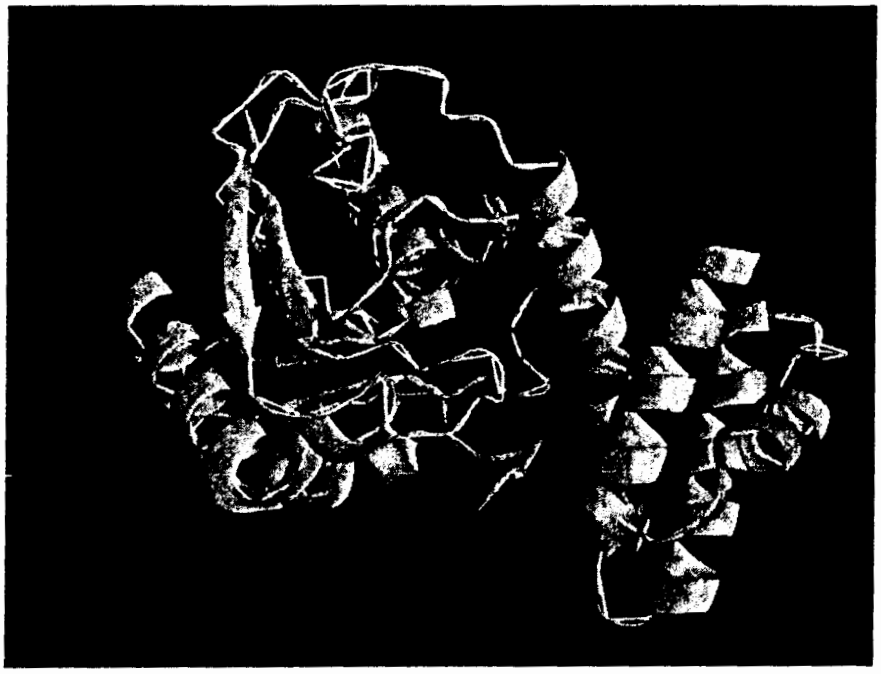

Figure 3. A TE9 tertiary structure.

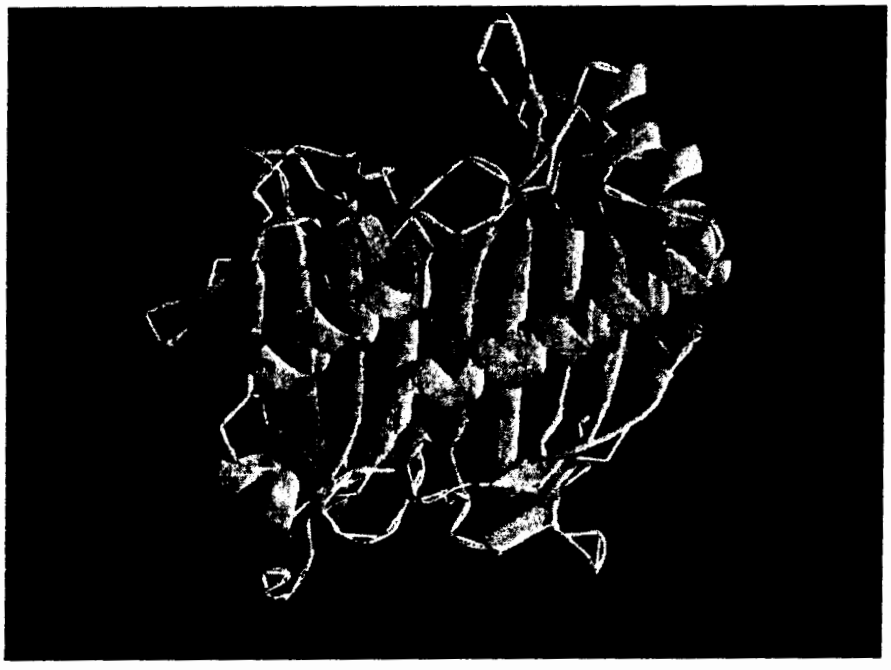

Figure 4. A TE12 tertiary structure with a double hotdog fold.

Figure 5. A TE13 tertiary structure.

Tailoring Polysaccharide-Based Nanostructured Biomaterials for Guided Mesenchymal Stem Cell (MSC) Response

Jorge Almodóvar[*], Matt J. Kipper[*,†]
[*]Department of Chemical and Biological Engineering, Colorado State University
[†]School of Biomedical Engineering, Colorado State University
1370 Campus Delivery, Fort Collins, CO 80523-1370

Abstract

It is generally accepted that both chemical and topographical cues affect mesenchymal stem cell (MSC) proliferation and differentiation. In our work, we have developed and characterized polysaccharide-based biomaterials with tailored nanostructures. Using the naturally-derived polysaccharides chitosan and hyaluronan we have constructed polyelectrolyte multilayers (PEMs). These polysaccharides are attractive biomaterials due to their biocompatibility, biodegradability, biochemical functionality, and antimicrobial properties. Currently our lab is pursuing *in vitro* studies to determine how MSCs might respond to the biochemical and topographical features that can be provided by nanostructured polysaccharide-based surface coatings. Here we report *in vitro* evaluations of MSC response to PEMs with different surface treatments. MSC proliferation studies have been performed for the PEM system. MSCs were seeded on PEMs constructed in tissue culture grade polystyrene dishes with and without fibronectin. The effect of cross-linking the PEMs using glutaraldehyde was also investigated. It was noted that the addition of fibronectin enhances the MSC proliferation rate. Cross-linking with glutaraldehyde hindered MSC proliferation. Further studies consist of delivering important growth factors to MSCs using polysaccharide-based PEMs.

Introduction

Bone marrow-derived MSCs are pluripotent stem cells that differentiate into different cell lineages in the presence of proper stimuli.[1] It has been demonstrated that nanoscale topographical features[2] and biochemical cues, such as growth factors[3] and polysaccharides,[4] induce controlled MSC differentiation. Adding nanoscale topographical features coupled with delivery of important proteins has the potential to greatly improve tissue-engineered implants and promote healthy tissue formation.

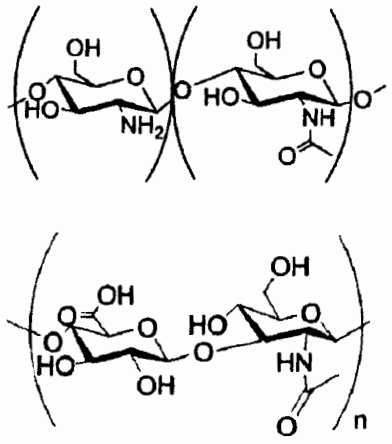

Figure 2. Chemical structure for the repeating units of chitosan (top) and hyaluronic acid (bottom).

In this work, the polyelectrolytes chitosan and hyaluronan were used to create PEMs, and MSC proliferation was assessed on PEMs with different conditions. Chitosan (CHI) (Figure 1) is a glycosaminoglycan-like weak polycation derived from the *N*-deacetylation of chitin, the most abundant naturally occurring polysaccharide.[5] Chitosan has been widely used in both the packaging industry[6] and the construction of vascular grafts[7] due to its antimicrobial activity. Chitosan-based scaffolds support mammalian cell growth, and therefore chitosan is an attractive material for wound healing applications.[8, 9] Pusateri *et al.* demonstrated that chitosan-based hemostatic dressings improve wound healing as a result of hepatic injury in swine.[10] Hyaluronan (HA) (Figure 1) is the only non-sulfated glycosaminoglycan, making it a weak polyanion of great biological interest. It serves as a lubricant in cartilage, participates in the control of tissue hydration and water transport, and in the control of the inflammatory response after trauma.[11] It has been used for the construction of PEMs[12] and hydrogels[5] for mammalian cell culture. Both of these polysaccharides are biodegradable, degrading into inert products such as di- and mono-saccharides (carbohydrates).

Other researchers have investigated mammalian cell behavior using polysaccharides and/or polyelectrolyte-based surfaces. Richert *et al.* found a decrease in chondrocyte attachment to chitosan-

hyaluronan PEMs with increasing numbers of bilayers.[12] Sechriest *et al.* noted that chondrocytes seeded in chitosan/chondroitin sulfate-A hydrogels assumed a spherical morphology, while the cells seeded in tissue-culture polystyrene (TCPS) assumed a fibroblastic morphology.[8] However, they noted that cell proliferation decreased almost 4-fold for the chondrocytes in the hydrogel. The addition of the protein fibronectin (FN) to polysaccharide-based surfaces has been demonstrated to improve cell adhesion and proliferation.[13] Fibronectin is a large protein found in the extracellular matrix, which regulates several cell functions, including cell attachment and cell spreading.[14]

In this article we report results obtained from the interactions between bone marrow derived MSCs and polysaccharide-based PEMs. PEMs were constructed to be either chitosan-terminated or hyaluronan-terminated. Three conditions were investigated: (1) un-modified PEMs, (2) PEMs with fibronectin adsorbed as the final layer, and (3) PEMs cross-linked with glutaraldehyde. Ovine MSCs were harvested and seeded on these surfaces using TCPS surfaces as a control. Cell counts and microscopic images were obtained at days 2 and 4.

Materials and Methods

Materials. Purified chitosan (4.7% acetylated) was purchased from Biosyntech Inc. (Laval, Canada). Hyaluronan sodium salt was purchased from Sigma-Aldrich (St. Louis, MO). Glacial acetic acid and glutaraldehyde (8% in water) were purchased from Acros Organics (Geel, Belgium). Sodium acetate was purchased from Fisher Scientific (Pittsburgh, PA). A Millipore Synthesis water purification unit was used to obtain 18.2 MΩ water, used for making all aqueous solutions (Millipore, Billerica, MA). The following were purchased from HyClone (Logan, UT): sterile fetal bovine serum (FBS); trypsin 0.25% with EDTA and 2.5 g of porcine trypsin; low glucose D-MEM media supplemented with 4 mM L-glutamine, 1 mg/mL glucose, and 110 mg/L sodium pyruvate; sterile alpha modification MEM media supplement with L-glutamine, ribonucleosides, and deoxyribonucleosides; and Dubelcco's phosphate buffered saline (DPBS) without Ca^{2+} and Mg^{2+}. The following were purchased from Gibco (Grand Island, NY): antibiotic-antimycotic (Anti/Anti), sterile HEPES buffer solution 1M, and Dulbecco's phosphate buffered saline with Ca^{2+} and Mg^{2+}. Fibronectin was purchased from BD Biosciences (Bedford, MA), and was used without further purification.

Cell harvest and culture. Bone marrow was harvested from the iliac crest of sheep, generously donated by Dr. Simon Turner in the Colorado State University College of Veterinary Medicine and Biomedical Sciences. The bone marrow was obtained shortly after the animal is euthanized. The skin area by the iliac crest of the sheep was exposed, cleaned, and then a bone marrow sample (2-4 ml) was obtained using a Jamshidi® biopsy needle (CardinalHealth, Dublin, OH) loaded with heparin at 1000 Units/ml (APP Pharmaceuticals, Schaumbirg, IL). The bone marrow was centrifuged at 200×g for 2-6 minutes to separate the MSCs from the rest of the marrow. The supernatant containing MSCs and red blood cells (RBCs) was extracted and the MSCs were counted after lysing the RBCs using ammonium chloride (0.15 M). The supernatant was placed in a T-25 culture flask (Corning, Lowell, MA) supplemented with growth media (low-glucose D-MEM with 10 % FBS, 1 % Anti/Anti, 2.5 % HEPES). The MSCs were allowed to adhere to the culture flask for 24 hours and then the floating RBCs were aspirated followed by a change of growth media. The MSCs were allowed to culture expand for at least 7 days until cell colonies were visible. After culture expansion, the cells were rinsed with DPBS without Ca^{2+} and Mg^{2+}, lifted using trypsin, counted using a hemocytometer (Bright-Line, Horsham, PA), and either re-seeded in culture flasks using maintenance media (α-MEM with 10% FBS, 1% Anti/Anti, 2.5% HEPES) or stored in a -80 °C freezer in freezing media (95 % FBS, 5 % dimethyl sulfoxide) until further use. The cells used in this study were in their third passage from three different female sheep no more that four years old.

Construction of polyelectrolyte multilayers on tissue culture polystyrene (TCPS) and cell seeding. Construction of the PEMs on TCPS was performed using sterile tissue culture polystyrene 12-

well Nuclon Δ surfaces (Nunc ALS, Roskilde, Denmark). Due to the already negative charge of TCPS, no further surface modification was needed. Chitosan and hyaluronan polyelectrolyte solutions with concentrations of 0.01 M (on a repeat unit basis) were prepared at pH 5.0 in 0.2 M acetate buffer. PEMs were constructed by alternating adsorption of polycationic chitosan and polyanionic hyaluronan using five-minute adsorption steps. A five-minute rinse step (water acidified to pH 4.0 using acetic acid) followed each adsorption step to remove unbound polyelectrolytes. The adsorption and rinse steps were conducted under agitation using a titer plate shaker (Thermo-Electron, Madison, WI), to improve mass transfer. X-ray photoelectron spectroscopy confirms the construction of these surfaces on the TCPS. (Data not shown.[15]) Three types of surfaces were prepared: un-modified PEMs, PEMs with fibronectin adsorbed as the final layer, and PEMs cross-linked using glutaraldehyde. Fibronectin was adsorbed from a DPBS with Ca^{2+} and Mg^{2+} solution at a concentration equivalent to 1.2 μg per cm^2 of culture surface. Glutaraldehyde cross-linking was performed by adding 1 ml of 2 % glutaraldehyde solution in water on the well for 30 minutes. The glutaraldehyde was removed and the wells were washed extensively. Triplicate experiments were performed for each surface treatment. Surfaces were sterilized using 70 % ethanol, and rinsed with Dubelcco's PBS prior to cell seeding. MSCs were seeded at a density of 5000 cells/cm^2 in maintenance media. MSCs were cultured for four days, with a change of media at the second day. At days 2 and 4 the cells were imaged and counted. The cells were imaged with a phase-contrast microscope using a 10x objective at the second and fourth days. Cell numbers were obtained for all conditions at the second and fourth days using a hemocytometer.

Results and Discussion

Figure 2 shows cell number for the different conditions investigated. In general it was observed that the MSCs were able to adhere and proliferate on polysaccharide based PEM. However, the control TCPS surfaces demonstrated more cell proliferation than any of the studied surfaces. Glutaraldehyde cross-linking negatively affects MSC proliferation. The addition of the glutaraldehyde most likely caused many cells to die. Presence of fibronectin enhanced MSC proliferation in chitosan-terminated PEMs, but it did not affect MSC proliferation in hyaluronan-terminated PEMs. This could be because little or no fribronectin was adsorbed onto the PEMs due to like charge repulsion. Fibronectin has an iso-electric point of 5.2[16] which will cause the protein to have an overall negative surface charge at physiological pH (7.3). This negative charge causes repulsion between the hyaluronan-terminated (negative) surfaces and the protein. However, chitosan (neutral at pH 7.3) provides a surface where fibronectin can be adsorbed. Fibronectin contains the RGD amino acid sequence which binds specifically to integrin receptors on mammalian cell membranes improving cell adhesion.[13] Fibronectin also has several binding sites for other extracellular matrix molecules including heparin, fibrin, and collagen.[17]

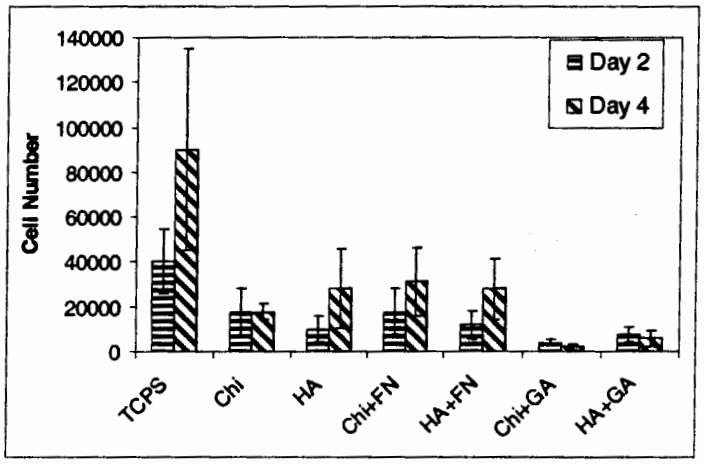

Figure 3. MSC proliferation data for chitosan (Chi), hyaluronic acid (HA) terminated surfaces treated with either fibronectin (FN) or glutaraldehyde (GA). Control surface was tissue-culture polystyrene (TCPS). Error bars represent standard deviation of triplicate experiments.

Phase-contrast micrographs (Figure 3) confirm the results presented in Figure 2. The enhancement in proliferation due to the addition of fibronectin can be clearly seen on the chitosan terminated surfaces, whereas the hyaluronan-terminated surfaces show little enhancement in cell proliferation even with the addition of fibronectin.

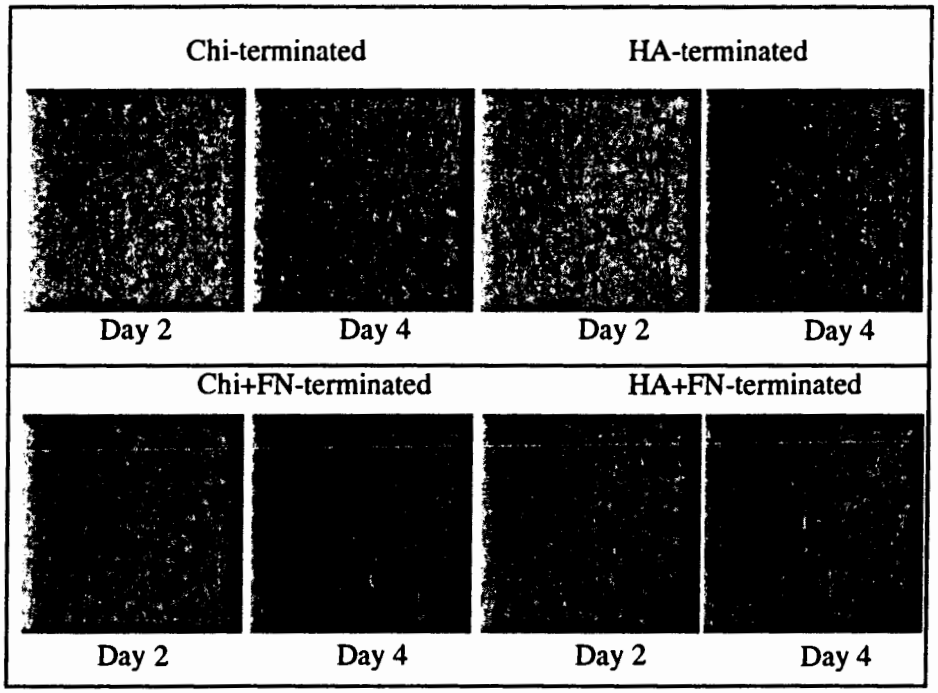

Figure 3. Phase-contrast micrographs for chitosan-terminated (Chi), and hyaluronan-terminated (HA) surfaces with and without fibronectin (FN).

Conclusions

These preliminary results indicate that while cell proliferation is hindered by the polysaccharide surfaces (when compared to TCPS), the surfaces are relatively non cyto-toxic. The addition of fibronectin seems to improve cell adhesion and proliferation on chitosan-terminated surfaces, while it has little effect on hyaluronan-terminated surfaces. As future work the interactions between PEMs and proteins will be assessed using IR spectroscopy for fibronectin and the growth factors TGF-β1, FGF-2, and BMP-2. The effects on MSC behavior of multiple growth factors (TGF-β1, FGF-2, BMP-2) adsorbed to or in PEMs and PCN will also be investigated.

Acknowledgements

We thank Dr. Simon Turner, Dr. John Kisiday, and Ben Hale for their assistance during the cell harvest.

References

1. Pittenger, M. F.; Mackay, A. M.; Beck, S. C.; Jaiswal, R. K.; Douglas, R.; Mosca, J. D.; Moorman, M. A.; Simonetti, D. W.; Craig, S.; Marshak, D. R., Multilineage potential of adult human mesenchymal stem cells. *Science* 1999, *284* (5411), 143-147.
2. Christenson, E. M.; Anseth, K. S.; van den Beucken, L.; Chan, C. K.; Ercan, B.; Jansen, J. A.; Laurencin, C. T.; Li, W. J.; Murugan, R.; Nair, L. S.; Ramakrishna, S.; Tuan, R. S.; Webster, T. J.; Mikos, A. G., Nanobiomaterial applications in orthopedics. *Journal of Orthopaedic Research* 2007, *25* (1), 11-22.
3. Liu, Y.; Enggist, L.; Kuffer, A. F.; Buser, D.; Hunziker, E. B., The influence of BMP-2 and its mode of delivery on the osteoconductivity of implant surfaces during the early phase of osseointegration. *Biomaterials* 2007, *28* (16), 2677-2686.
4. Park, J. S.; Woo, D. G.; Yang, H. N.; Lim, H. J.; Chung, H. M.; Park, K. H., Heparin-bound transforming growth factor-beta 3 enhances neocartilage formation by rabbit mesenchymal stem cells.

Transplantation 2008, *85* (4), 589-596; Abarrategi, A.; Civantos, A.; Ramos, V.; Casado, J. V. S.; Lopez-Lacomba, J. L., Chitosan film as rhBMP2 carrier: Delivery properties for bone tissue application. *Biomacromolecules* 2008, *9* (2), 711-718.

5. Suh, J. K. F.; Matthew, H. W. T., Application of chitosan-based polysaccharide biomaterials in cartilage tissue engineering: a review. *Biomaterials* 2000, *21* (24), 2589-2598.
6. Durango, A. M.; Soares, N. F. F.; Benevides, S.; Teixeira, J.; Carvalho, M.; Wobeto, C.; Andrade, N. J., Development and evaluation of an edible antimicrobial film based on yam starch and chitosan. *Packaging Technology and Science* 2006, *19* (1), 55-59; Lee, C. H.; An, D. S.; Park, H. F.; Lee, D. S., Wide-spectrum antimicrobial packaging materials incorporating nisin and chitosan in the coating. *Packaging Technology and Science* 2003, *16* (3), 99-106.
7. Fujita, M.; Kinoshita, M.; Ishihara, M.; Kanatani, Y.; Morimoto, Y.; Simizu, M.; Ishizuka, T.; Saito, Y.; Yura, H.; Matsui, T.; Takase, B.; Hattori, H.; Kikuchi, M.; Maehara, T., Inhibition of vascular prosthetic graft infection using a photocrosslinkable chitosan hydrogel. *Journal of Surgical Research* 2004, *121* (1), 135-140; Hu, S. G.; Jou, C. H.; Yang, M. C., Surface grafting of polyester fiber with chitosan and the antibacterial activity of pathogenic bacteria. *Journal of Applied Polymer Science* 2002, *86* (12), 2977-2983.
8. Sechriest, V. F.; Miao, Y. J.; Niyibizi, C.; Westerhausen-Larson, A.; Matthew, H. W.; Evans, C. H.; Fu, F. H.; Suh, J. K., GAG-augmented polysaccharide hydrogel: A novel biocompatible and biodegradable material to support chondrogenesis. *Journal of Biomedical Materials Research* 2000, *49* (4), 534-541.
9. Raghunath, J.; Rollo, J.; Sales, K. M.; Butler, P. E.; Seifalian, A. M., Biomaterials and scaffold design: key to tissue-engineering cartilage. *Biotechnology and Applied Biochemistry* 2007, *46*, 73-84.
10. Pusateri, A. E.; McCarthy, S. J.; Gregory, K. W.; Harris, R. A.; Cardenas, L.; McManus, A. T.; Goodwin, C. W., Effect of a chitosan-based hemostatic dressing on blood loss and survival in a model of severe venous hemorrhage and hepatic injury in swine. *Journal of Trauma-Injury Infection and Critical Care* 2003, *54* (1), 177-182.
11. Lapcik, L.; De Smedt, S.; Demeester, J.; Chabrecek, P., Hyaluronan: Preparation, structure, properties, and applications. *Chemical Reviews* 1998, *98* (8), 2663-2684; Laurent, T. C.; Fraser, J. R. E., HYALURONAN. *Faseb Journal* 1992, *6* (7), 2397-2404.
12. Richert, L.; Lavalle, P.; Payan, E.; Shu, X. Z.; Prestwich, G. D.; Stoltz, J. F.; Schaaf, P.; Voegel, J. C.; Picart, C., Layer by layer buildup of polysaccharide films: Physical chemistry and cellular adhesion aspects. *Langmuir* 2004, *20* (2), 448-458.
13. Wittmer, C. R.; Phelps, J. A.; Saltzman, W. M.; Van Tassel, P. R., Fibronectin terminated multilayer films: Protein adsorption and cell attachment studies. *Biomaterials* 2007, *28* (5), 851-860.
14. Osaki, T.; Renner, L.; Herklotz, M.; Werner, C., Hydrophobic and electrostatic interactions in the adsorption of fibronectin at maleic acid copolymer films. *Journal of Physical Chemistry B* 2006, *110* (24), 12119-12124.
15. Boddohi, S.; Almodovar, J.; Zhang, H.; Johnson, P.; Kipper, M., Fabrication and characterization of polysaccharide-based nanostructured surfaces prepared with polyelectrolyte complex nanoparticles. *Langmuir (Submitted)* 2009.
16. Tooney, N. M.; Mosesson, M. W.; Amrani, D. L.; Hainfeld, J. F.; Wall, J. S., SOLUTION AND SURFACE EFFECTS ON PLASMA FIBRONECTIN STRUCTURE. *Journal of Cell Biology* 1983, *97* (6), 1686-1692.
17. Shirley, A.; P., B.-H. R.; J., H. M.; E., K. K.; Adrian, S. C., *The Extracellular Matrix FactsBook*. Academic Press: San Diego, 1998.

Nanoassembly of polysaccharide based polyelectrolytes: Tuning morphology and Size

Soheil Boddohi[†], Jorge Almodóvar[†], Hao Zhang[‡], Patrick A. Johnson[‡], and Matt J. Kipper[†,§]
[†]Department of Chemical and Biological Engineering, Colorado State University, Fort Collins CO 80523-1370, [‡]Department of Chemical and Petroleum Engineering, University of Wyoming, Laramie WY, 82071, [§]School of Biomedical Engineering, Colorado State University, Fort Collins CO, 80523-1370

Abstract

Nanoassembly of polysaccharides using polyelectrolyte multilayers (PEMs), polyelectrolyte complex nanoparticles (PCNs), and combinations of these two nanostructures was demonstrated. The polysaccharides used in PEM and PCN formation were chitosan, heparin, and hyaluronan. The aim of this work was to demonstrate that the topography and composition of polysaccharide-based surface coatings can be tuned at the nanoscale. The construction of PEMs was monitored *in situ* using Fourier-transform surface plasmon resonance (FT-SPR) at different values of solution pH and buffer molarity. PCNs were formed by complexation of oppositely charged polyelectrolytes in different charge mixing ratios. PCNs were characterized by dynamic light scattering (DLS) to determine the size distributions. Nanostructured surface coatings were characterized on both modified gold substrates and tissue-culture polystyrene surfaces. When PCNs were introduced into PEMs, the formation of the surface coatings was monitored by *in situ* quartz crystal microbalance with dissipation (QCM-D) experiments. Surface topography was characterized by scanning electron microscopy (SEM) and atomic force microscopy (AFM). Surface chemistry was confirmed by both vibrational spectroscopy and X-ray photoelectron spectroscopy. PCNs were adsorbed to oppositely charged PEMs, and were also embedded within PEMs. We demonstrate that PEM thickness can be controlled with nanometer resolution by altering the deposition conditions (changing buffer pH and molarity and number of layers). The size distributions of PCNs can be altered by changing the charge mixing ratios of the two constituent polyelectrolytes. We demonstrate that PCNs were colloidally stable and homogenously distributed when adsorbed on or in the PEMs. PCNs introduce surface features ranging from 80 nm to 250 nm in width and 15 nm to 30 nm in height. The combination of polyelectrolyte complex nanoparticle formation and polyelectrolyte multilayer formation can be used to tune the nanoscale topographical features and composition of polysaccharide-based ultra thin films.

Introduction

Layer-by-layer assembly (LBL) of oppositely charged polyelectrolytes is a simple and reproducible technique that can be used to form ultra thin polymer films. It has been used for the fabrication of functional nanoscale coatings on solid surfaces like gold, glass, or silicon.[1,2] LBL assembly of polyelectrolyte multilayers (PEMs) of synthetic polymers has been studied extensively and has revealed some dependence on experimental parameters like pH, ionic strength, and polymer charge density.[3,4] The pH dependence of PEM assembly using weak polyelectrolytes has also been investigated by several groups.[5,6]

Polyelectrolyte complexation in solution can also be used to form nanoparticles. Polyelectrolyte complex nanoparticles (PCNs) were first characterized by Tsuchida and Kabanov.[7-11] When oppositely charged polyelectrolytes complex in solution with one of the constituent charged groups in excess, both positively charged and negatively charged colloidal nanoparticles can be formed, stabilized by excess surface charge.[12] Many parameters can influence the mechanism of PCN formation, and the resulting particle size, composition, and stability. These parameters include the charge mixing ratio of oppositely charged polymers, charge density of polyelectrolytes, polymer size, and properties of the polyelectrolyte solutions.

Nanoscale surface features can influence the biological response of mammalian cells cultured on nanostructured biomaterials.[13] Thus, decorating charged surfaces with nanoparticles is a method that can enable one to tailor the nanoscale morphology and composition of surface coatings to influence the biological response to materials. Adsorption of organic and inorganic nanoparticles during PEM

formation has been investigated by several groups.[14-17] We have previously reported on the adsorption of polysaccharide-based PCNs to surfaces. In this work however, we were not able to achieve control over the surface adsorption to the extent of obtaining uniform surface coverage or preventing particle aggregation for all conditions studied.[18]

Biologically derived polysaccharides, many of which are polyelectrolytes, have great potential in a number of biomedical applications, including as biochemically active materials for tissue engineering scaffolds. Chitosan as a weak polycation with a pKa 6.46 to7.32 is insoluble in most solvents but soluble in aqueous solution below its pKa.[19,20] Chitosan has shown some antimicrobial activity, biocompatibility, and potential to promote wound healing.[21-23] Heparin has the highest negative charge density of any known biological polyanion due to its sulfate and carboxylate substituents. Heparin has many different sequences that can bind to different growth factors including insulin-like growth factor, fibroblast growth factors, and members of the transforming growth factor beta super family.[24-26] Hyaluronan is a weak polyanion that plays important roles in organizing proteins in the extra cellular matrix. It is one of the important components of joint tissues and influences cell migration and proliferation.

In this article, we demonstrate that chitosan-heparin and chitosan-hyaluronan PEMs and PCNs were successfully made. In our previous work, chitosan-heparin PEMs were extensively characterized by vibrational spectroscopy and optical techniques.[27] In other work by our group, chitosan-heparin and chitosan-hyaluronan nanoparticles were also characterized by dynamic light scattering (DLS) and scanning electron microscopy (SEM).[18] In the current work we summarize this previous work and also report on the surface coating of chitosan-hyaluronan PEMs containing chitosan-heparin PCNs.

Materials and Methods

Materials. Purified chitosan (4.7% acetylated) was purchased from Biosyntech Inc. (Laval, Canada). Heparin sodium (from porcine intestinal mucosa, 12.5% sulfur) was purchased from Celsus Laboratories (Cincinnati, OH). Hyaluronan sodium salt and 11-mercaptoundecanoic acid were purchased from Sigma-Aldrich (St. Louis, MO). Glacial acetic acid and ethanol (200 proof 99.5+ %) were purchased from Acros Organics (Geel, Belgium). Sodium acetate was purchased from Fisher Scientific (Pittsburgh, PA). A Millipore Synthesis water purification unit was used to obtain 18.2 MΩ water, used for making all aqueous solutions (Millipore, Billerica, MA).

LBL assembly and in situ Fourier-transform surface plasmon resonance (FT-SPR). PEMs were formed on gold-coated SF-10 glass substrates (GWC Technologies Inc., Madison WI) modified with a self-assembled monolayer of 11-mercaptoundecanoic acid. LBL assembly of PEMs was conducted in the flow cell of an SPR-100 module coupled to a Nicolet 8700 FT-IR spectrometer (Thermo-Electron, Madison, WI). Data were collected using the Omnic 7.3 software (Thermo Electron), at 8 cm^{-1} resolution over the range from 6000 to 12,000 cm^{-1}. 16 scans were co-added at each time point to produce an FT-SPR spectrum every 4.7 seconds.

Substrates were first exposed to a rinse solution (18.2 MΩ water acidified to pH 4.0 with acetic acid). PEMs were then produced by alternately exposing the substrate to the respective solutions of polycation and polyanion for 5 min. The substrates were rinsed for 5 min between each adsorption step. Ten–layer PEMs were assembled from acetate buffer solutions over the pH range of 4.6 to 5.8 at 0.1, 0.2, and 0.5 M. Duplicate PEM were prepared from fresh solutions at each combination of pH and ionic strength studied.

PCN Preparation. Chitosan, heparin, and hyaluronan solutions were prepared at concentrations of 0.9 mg mL^{-1} , 0.95 mg mL^{-1}, and 1mg/ mL^{-1} respectively, in acetate buffer solution (pH 5, 0.1 M). PCNs were formed by the one-shot addition of the polyelectrolyte in default to the polyelectrolyte in excess, to create a total volume of 10 mL. The mixture was stirred for 3 hours at 800 rpm. Particles were then centrifuged, after allowing aggregates to settle overnight, and PCNs were resuspended in 10 mL of pH 5.0, 0.1 M acetate buffer.

Dynamic light scattering (DLS). A DynaPro Titan (Wyatt Technologies, Santa Barbara, CA) instrument was used to perform DLS, using an 830-nm laser. All measurements were performed at a fixed

angle of 90° at 25 °C. Five measurements of 50 s each were performed for each 10-μL sample of suspended PCNs.

Construction of PCN-containing PEMs on modified gold surfaces and tissue culture polystyrene (TCPS). Nanostructured surfaces described in Table 1 were constructed on two different types of gold-coated substrates using similar techniques: AT-cut piezoelectric gold-coated sensor crystals (Q-Sense, Inc. Glen Burnie, MD) and glass slides prepared by coating with an adhesion layer of chromium, followed by gold. Gold surfaces were then modified with an 11-mercaptoundecanoic acid self-assembled monolayer (MUA SAM). Layer-by-layer assembly of the surface coatings was conducted on the QCM-D crystals in a Q-Sense E4™ quartz crystal microbalance with dissipation monitoring (QCM-D) system (Q-Sense, Inc.). Construction of the PEMs and PCN-containing PEMs described on Table 1 on TCPS was also performed using sterile tissue culture polystyrene 6-well Nunclon Δ surfaces (Nunc ALS, Roskilde, Denmark). The adsorption and rinse steps were conducted under agitation using a vortexer, to improve mass transfer. For construction of all surfaces chitosan and hyaluronan polyelectrolyte solutions with concentrations of 0.01 M (on a repeat unit basis) were prepared at pH 5.0 in 0.2 M acetate buffer.

Scanning electron microscopy (SEM). The shape and size of features on the PCN-containing PEMs were investigated by SEM using a JEOL JSM-6500F field emission scanning electron microscope (Jeol, Peabody, MA). Images at four different magnifications (330×, 1000×, 3300×, 10000×, and 33000×) were collected for each sample.

Atomic force microscopy (AFM). The surface morphology of the nanostructured coatings was investigated using a Nanosurf Easyscan 2 AFM (Fort Lee, NJ) and PPP-NCLR-50 tips from Nanosensors (Switzerland). Micrographs were obtained using tapping mode. Image analysis was performed using the Scanning Image Probe Processor version 4.2.2.0 software. Samples were prepared on the nanosensor gold crystals by QCM-D and TCPS substrates. AFM was performed at room temperature in air at a rate of one line scan per second.

Results and Discussion

Formation of polysaccharide-based PEMs. Chitosan-heparin PEMs were built up using FT-SPR from solutions at 4 different pH values, ranging from 4.6 to 5.8, and three different buffer molarities. *In situ* thicknesses for chitosan-heparin PEMs were determined assuming their refractive index is 1.41 (determined from spectroscopic ellipsometry), and using multiphase Fresnel calculations to model the plasmon resonance peak position as a function of PEM thickness. Figure 1 shows PEM thicknesses versus layer number. Layer zero is the MUA SAM; odd-numbered and even-numbered layers represent the chitosan layers and heparin layers respectively. For the 0.2 M buffer (Figure 1b), the broadest range of accessible PEM thickness is obtained by modulating the solution pH. At lower pH, the chitosan has a higher charge density, and a more extended conformation in solution, potentially leading to thinner layers upon adsorption. At elevated pH the chitosan becomes increasingly hydrophobic, this corresponds to a collapse in solution and requires more polymer to adsorb in order to invert the surface charge at each chitosan adsorption step, leading to thicker layers. When the buffer molarity is reduced to 0.1 M (Figure 1a) or increased to 0.5 M (Figure 1c), the effects due to pH change are less pronounced. This could be because the 0.1 M buffer has reduced buffering capacity and the 0.5 M buffer has increased electrostatic screening

Characterization of PCN: Size and morphology. Oppositely charged polyelectrolytes were complexed electrostatically in solution in different mixing ratios. Chitosan-heparin and chitosan-hyaluronan pairs formed nanoparticles in mixing ratios ranging from 0.08 to 19.2. The hydrodynamic radius of the particles in solution measured using DLS was in the range of 150 to 250 nm. Figure 2a and Figure 2b show the size distributions for different charge mixing ratios of the chitosan-heparin PCNs for negatively charged and positively charged particles, respectively. In figure 3c, R_H versus charge mixing ratios is shown. Making particles close to the 1:1 charge mixing ratio was not possible and results in aggregate formation due to the lower colloidal stability of the particles. Farther from the 1:1 charge

mixing ratio, particles tend to be more stable due to their increase in net charge, enabling smaller particles to be formed. Data for chitosan-hyaluronan nanoparticles are not shown..

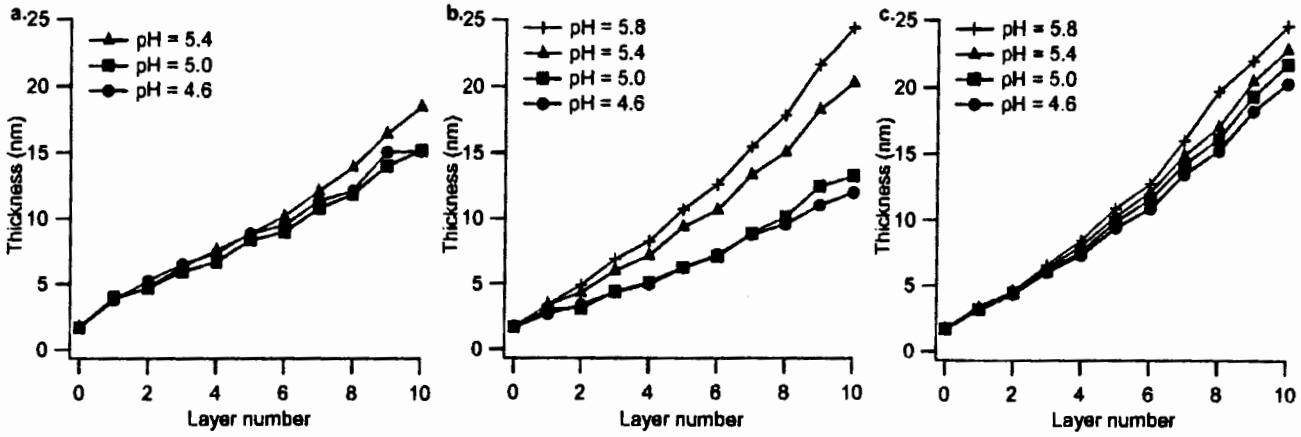

Figure 1. PEM thickness obtained from *in situ* FT-SPR data as a function of layer number and pH for 0.1 M buffer (a), 0.2 M buffer (b), and 0.5 M buffer (c). In all three plots, layer zero represents the MUA SAM thickness (1.7 nm). Odd-numbered layers are chitosan and even-numbered layers are heparin. Data for each condition are the averages of two replicate experiments. Reprinted with permission from Boddohi *et al.*, *Biomacromolecules* 9 (7), pp 2021–2028. Copyright 2008 American Chemical Society.

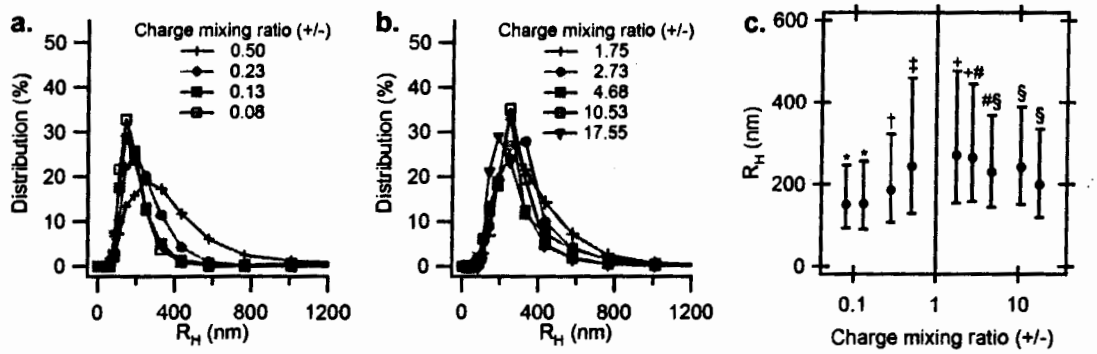

Figure 2. Size distributions for negatively charged (a.) and positively charged (b.) chitosan-heparin PCN obtained by DLS in different mixing ratios. Figure1c represents hydrodynamic radii versus charge mixing ratios for all conditions. In c., the data marked with symbols are statistically different ($p < 0.05$) from data not marked with the same symbol. (Comparisons were only made among particles with like charge, i.e. charge mixing ratio either greater than or less than 1.) Reprinted with permission from Boddohi *et al.*, *Biomacromolecules*, 10 (6), pp 1402–1409. Copyright 2009, American Chemical Society.

Characterization of PCN-containing PEMs. Chitosan-hyaluronan PEMs were formed on QCM-D crystals to measure the polymer mass adsorbed at each adsorption step. The eight different conditions studied are described in Table 1. The notation m_6 and m_7 refer to six-layer and seven-layer chitosan-hyaluronan PEMs. The m_6 surface is terminated with hyaluronan, while the m_7 surface is terminated with chitosan. m_6p^-, m_6p^+, m_7p^+, and m_7p^- refer to either a hyaluronan- or chitosan-terminated PEMs to which either positively charged (p^+) or negatively charged (p^-) PCNs were subsequently adsorbed. $m_6p^+m_6$ and $m_7p^-m_6$ refer to PEMs with PCNs adsorbed followed by an additional six layers of polymer. For both of these conditions, the layer immediately following the PCN adsorption step is the polyelectrolyte with the same charge as the PCNs. The final masses adsorbed for each condition are reported in Table 1. Note that when the PCNs adsorbed have the same charge as the terminal layer of the PEMs, very little mass

difference is obtained compared to the masses of the underlying PEMs. However, a much larger mass difference is achieved when the charge of the PCNs is opposite of the charge on the underlying PEMs. The data in Table 1 also demonstrate that multilayers can be successfully added on top of PCN-modified PEMs.

Table 1. Surface conditions for PEM-PCN modifications.

Sample name	Surface condition	Mass (ng/cm^2)
m_6	$(chi\text{-}ha)_3$	1129
m_6p^-	$(chi\text{-}ha)_3\text{-}(PCN)^-$	1243
m_6p^+	$(chi\text{-}ha)_3\text{-}(PCN)^+$	1360
$m_6p^+m_6$	$(chi\text{-}ha)_3\text{-}(PCN)^+\text{-}(chi\text{-}ha)_3$	3068
Sample name	**Surface condition**	**Mass (ng/cm^2)**
m_7	$(chi\text{-}ha)_3\text{-}chi$	1310
m_7p^+	$(chi\text{-}ha)_3\text{-}chi\text{-}(PCN)^+$	1355
m_7p^-	$(chi\text{-}ha)_3\text{-}chi\text{-}(PCN)^-$	1835
$m_7p^-m_6$	$(chi\text{-}ha)_3\text{-}chi\text{-}(PCN)^-\text{-}(ha\text{-}chi)_3$	3529

Figure 3a shows the mass adsorbed versus layer number for the $m_6p^+m_6$ and the $m_7p^-m_6$ surface coatings. In each data series, the un-filled data point represents the adsorption of the PCNs. The layer immediately following this data point represents adsorption of the polyelectrolyte that has the same charge as the subsequently adsorbed PCNs. Figures 3b and 3c show representative SEM images of the samples described in Table 1 (the m_6 and the m_6p^+ surfaces.

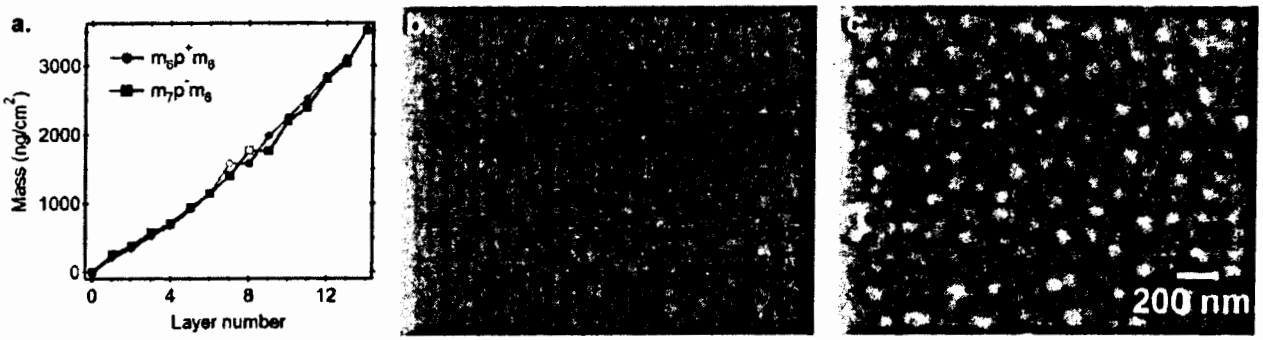

Figure 3. QCM-D data showing the change in mass per area as a function of time during the construction of the $m_6p^+m_6$ and the $m_7p^-m_6$ surface coatings (a.). In (a) the filled symbols represent polyelectrolyte adsorption steps and the open symbols represent PCN adsorption steps. Scanning electron micrographs of the m_6 and m_6p^+ surface coatings (b. and c.). The scale bar in (b.) applies to both (b.) and (c.)

Note that the polyelectrolyte layer immediately following the PCN adsorption shows no additional mass. This confirms that the PCNs completely cover the surface, preventing the like-charged polyelectrolyte from adsorbing. X-ray photoelectron spectroscopy and polarization modulation infrared reflection absorption spectroscopy were used to characterize the chemistry of the nanostructured surface coatings (data not shown). These chemical analyses confirmed that the features observed in Figure 3 represent changes in the surface chemistry (addition of sulfur) consistent with addition of heparin-containing PCNs to the surfaces. Atomic force microscopy was used to measure the size of the surface features introduced by the PCN adsorption. PEMs containing no PCNs exhibit surface roughness features generally less than 10 nm. After addition of PCNs, the surfaces are dominated by features from 15 to 40

nm in height and 80 to 250 nm in width. (AFM data not shown.) Similar results were obtained for surfaces constructed on TCPS surfaces.

Conclusions

We have demonstrated the construction of nanostructured polysaccharide-based surfaces. Formation of PEMs was characterized at different values of buffer pH and molarity. Formation of PCNs using both the chitosan-heparin and chitosan-hyaluronan polyelectrolyte pairs was also demonstrated. PCN size distributions were determined by DLS at different charge mixing ratios. PEMs and PCNs were successfully combined to introduce nanoscale surface topographical features and nanoscale regions of different surface chemistry into the polysaccharide-based surface coatings.

References

1. G. Decher, J.D. Hong, Buildup of ultrathin multilayer films by a self-assembly process .2. Consecutive adsoption of anionic and cationic bipolar amphiphilies and polyelectrolytes on charged surfaces, *Berichte Der Bunsen-Gesellschaft-Physical Chemistry Chemical Physics* **95**: 1430-1434 (1991).
2. G. Decher, Polyelectrolyte multilayers, an overview, in *Multilayer Thin Films Sequential Essembly of Nanocomposite Materials*, G. Decher, J. B. Schlenoff, Eds. (Wiley-VCH Verlag GmbH & Co., Weinheim, 2003), pp. 1-46.
3. J. Hiller, M.F. Rubner, Reversible molecular memory and pH-switchable swelling transitions in polyelectrolyte multilayers, *Macromolecules* **36**: 4078-4083 (2003).
4. J. Choi, M.F. Rubner, Influence of the degree of ionization on weak polyelectrolyte multilayer assembly, *Macromolecules* **38**: 116-124 (2005).
5. S.E. Morgan, P. Jones, A.S. Lamont, A. Heidenreich, C.L. McCormick, Layer-by-layer assembly of pH-responsive, compositionally controlled (co)polyelectrolytes synthesized via RAFT, *Langmuir* **23**: 230-240 (2007).
6. S.S. Shiratori, M.F. Rubner, pH-dependent thickness behavior of sequentially adsorbed layers of weak polyelectrolytes, *Macromolecules* **33**: 4213-4219 (2000).
7. E. Tsuchida, Y. Osada, K. Sanada, Interaction of poly(styrene sulfonate) with polycations carrying charges in the chain backbone, *J Polym Sci Polym Chem Ed* **10**: 3397-3404 (1972).
8. E. Tsuchida, Y. Osada, H. Ohno, Formation of intepolymer complexes, *Journal of Macromolecular Science-Physics* **B17**: 683-714 (1980).
9. V.A. Izumrudov, O.A. Kharenko, A.V. Kharenko, Z.G. Gulyaeva, V.A. Kasaikin, A.B. Zezin, V.A. Kabanov, Behavior of nonstoichiometric poly-electrolyte complexes in aqueous salts solutions, *Vysokomolekulyarnye Soedineniya Seriya A* **22**: 692-699 (1980).
10. V. Kabanov, A. Zezin, Soluble interpolymeric complexes as a new class of synthetic polyelectrolytes, *Pure Appl Chem* **56**: 343-354 (1984).
11. A.B. Zezin, V.A. Kabanov, New form of the poly-electrolytes water-soluble complexes, *Uspekhi Khimii* **51**: 1447-1483 (1982).
12. A.F. Thunemann, M. Muller, H. Dautzenberg, J.F.O. Joanny, H. Lowne, Polyelectrolyte complexes, *Adv Polym Sci* **166**: 113-171 (2004).
13. D.S. Kommireddy, I. Ichinose, Y.M. Lvov, D.K. Mills, Nanoparticle Multilayers: Surface Modification for Cell Attachment and Growth, *Journal of Biomedical Nanotechnology* **1**: 286-290 (2005).
14. D. Grigoriev, D. Gorin, G.B. Sukhorukov, A. Yashchenok, E. Maltseva, H. Mohwald, Polyelectrolyte/magnetite nanoparticle multilayers: Preparation and structure characterization, *Langmuir* **23**: 12388-12396 (2007).
15. Q. Li, J.F. Quinn, Y.J. Wang, F. Caruso, Preparation of nanoporous polyelectrolyte multilayer films via nanoparticle templating, *Chemistry of Materials* **18**: 5480-5485 (2006).

16. G. Bogdanovic, T. Sennerfors, B. Zhmud, F. Tiberg, Formation and structure of polyelectrolyte and nanoparticle multilayers: Effect of particle characteristics, *Journal of Colloid and Interface Science* **255**: 44-51 (2002).
17. T. Reihs, M. Müller, K. Lunkwitz, Preparation and adsorption of refined polyelectrolyte complex nanoparticles, *J Colloid Interface Sci* **271**: 69-79 (2004).
18. S. Boddohi, N. Moore, P.A. Johnson, M.J. Kipper, Polysaccharide-based polyelectrolyte complex nanoparticles from chitosan, heparin, and hyaluronan, *Biomacromolecules* **10**: 1402-1409 (2009).
19. W. Ding, Q. Lian, R.J. Samuels, M.B. Polk, Synthesis and characterization of a novel derivative of chitosan, *Polymer* **44**: 547-556 (2003).
20. V.M. Ramos, N.M. Rodriguez, M.S. Rodriguez, A. Heras, E. Agullo, Modified chitosan carrying phosphonic and alkyl groups, *Carbohydr Polym* **51**: 425-429 (2003).
21. X.F. Liu, Y.L. Guan, D.Z. Yang, Z. Li, K. De Yao, Antibacterial action of chitosan and carboxymethylated chitosan, *Journal of Applied Polymer Science* **79**: 1324-1335 (2001).
22. S.G. Hu, C.H. Jou, M.C. Yang, Surface grafting of polyester fiber with chitosan and the antibacterial activity of pathogenic bacteria, *Journal of Applied Polymer Science* **86**: 2977-2983 (2002).
23. J.K.F. Suh, H.W.T. Matthew, Application of chitosan-based polysaccharide biomaterials in cartilage tissue engineering: a review, *Biomaterials* **21**: 2589-2598 (2000).
24. S. Guimond, M. Maccarana, B.B. Olwin, U. Lindahl, A.C. Rapraeger, Activating and Inhibitory Heparin Sequences for FGF-2 (Basic FGF) - Distinct Requirements for FGF-1, FGF-2, and FGF-4, *J Biol Chem* **268**: 23906-23914 (1993).
25. M. Maccarana, U. Lindahl, Minimal sequence in heparin heparin-sulfate required for binding of basic fibroblast growth-factor, *Glycoconjugate Journal* **10**: 254-254 (1993).
26. B.H. Zhao, T. Katagiri, H. Toyoda, T. Takada, T. Yanai, T. Fukuda, U.I. Chung, T. Koike, K. Takaoka, R. Kamijo, Heparin potentiates the in vivo ectopic bone formation induced by bone morphogenetic protein-2, *Journal of Biological Chemistry* **281**: 23246-23253 (2006).
27. S. Boddohi, C.E. Killingsworth, M.J. Kipper, Polyelectrolyte multilayer assembly as a function of pH and ionic strength using the polysaccharides chitosan and heparin., *Biomacromolecules* **9**: 2021-2028 (2008).

Vertical Cell Assembly of Colloidal Crystal Films for Making Inverse Colloidal Crystal Membrane: A New Generation Ultrafiltration Membrane for Protein Separation

Xinying Wang [a], Scott M. Husson [b], Xianghong Qian [c], S. Ranil Wickramasinghe [a*]

[a] Department of Chemical and Biological Engineering, Colorado State University, Fort Collins, CO 80523, USA, wickram@engr.colostate.edu

[b] Department of Chemical and Biomolecular Engineering, Clemson University, Clemson, SC 29634, USA, shusson@clemson.edu

[c] Department of Mechanical Engineering, Colorado State University, Fort Collins, CO 80523, USA, xhqian@engr.colostate.edu

Abstract

Formation of colloidal crystal films (CCFs) is the first step in the fabrication of inverse colloidal crystals, a class of three-dimensionally ordered, macroporous materials. A new vertical cell assembly method is described that yields ICC membranes with area up to 500 mm^2. The cell consists of two microscope cover glasses separated by a thin polymeric spacer. The lower edge of the cell is placed in a colloidal dispersion. Particles are transported to the top of the cell by capillary force and self-assemble into CCF as the solvent evaporates. This novel vertical cell assembly method is well suited for fabrication of large-area CCFs with controllable thickness.

1. Introduction

Colloidal crystals (photonic crystals) are highly-ordered, three-dimensional structures of close-packed, uniform spheres. Natural opals are an example of colloidal crystals. Photonic crystals display a dielectric constant that varies with a periodicity similar to that of visible light resulting in a partial photonic band gap[1]. Consequently, they are of great interest as photonic band gap materials[2,3]. Colloidal crystal films (CCFs) may be processed into inverse colloidal crystals (ICCs), which are three-dimensionally ordered macroporous structures, where air fills the spaces originally occupied by the colloidal particles. ICCs could potentially display a complete photonic band gap, as they meet the theoretical requirement that the ratio of the maximum to minimum refractive index within the material be more than 2.9 for materials with high refractive indices such as Si and Ge. Thus, ICCs are also of great interest in photonics [2, 4, 5, 6, 7]. Production of defect-free CCFs is essential in order to fabricate ICC films that are suited ideally for size based filtration applications. Unfortunately, fabrication of large area, defect-free CCFs is often problematic[8]. Here, we describe an ICC membrane formation process that results in integral ICC membranes suitable for protein ultrafiltration.

2. Material and methods

Uniform polystyrene spheres with diameters of 423, 994 and 1998 nm and silicon dioxide particles with 400nm were used to fabricate CCFs. The polystyrene spheres with 423 nm particles were prepared according to Ceska et al.[9] The 994 and 1998 nm particles were purchased from Duke Scientific. The silicon dioxide particles were lab-made according to according to the Stober-Fink-Bohn method[10].

All particles were produced or received as an aqueous suspension. Prior to use, they were centrifuged at 6000 rpm for 10 min and washed with ethanol three times. Particles were resuspended in ethanol.

The vertical cell used to form the CCFs comprised two microscope cover glasses separated by two strips of Mylar film (Grafix, USA) (shaded strips in Fig. 1 (A)). The cell was held together by a clip at the bottom and placed vertically in a beaker (30 mL) that contained the

dispersion (20 mL) of polystyrene spheres in ethanol. The dispersions of polystyrene spheres with 423, 994 and 1998 nm were 15, 4 and 6 wt %, respectively the dispersion of silicon dioxide particles is 1-5%. The spheres were transported to the top of the vertical cell by capillary forces (Fig. 1 (A)). As the ethanol evaporated, the particles self assembled in the vertical cell over a 5-7 day period.

After formation of the colloidal crystal template, the template was dried at room temperature and infiltrated with the monomer solution consisting of 20 wt%2-hydroxyethyl methacrylate (Aldrich, 97%), 70 wt% hydroxybutyl methacrylate, mixture of isomers (Aldrich, 94%);, 8 wt% Ethylene glycol dimethacrylate (Aldrich, 98%) and 2 wt% benzoin isobutyl ether (Aldrich, 90%). The casting cell was irradiated with UV light to polymerize the monomers. The resulting colloidal crystal template was immersed into 10 wt% %); hydrofluoric acid (Aldrich, 40%) solution to etch away the template and the microscope slides.

ICC membranes and CCFs were coated with gold and imaged using Field Emission SEM (FESEM, JSM-6500F, JEOL, Japan).

3. Results and discussion

Using the vertical cell shown in Fig. 1 (A) we fabricated CCFs ranging from 25-100 μm in thickness by varying the thickness of the polymer spacer. Fig. 1 (B-D) are photographs of CCFs fabricated from 423, 994 and 1998 nm polystyrene spheres with spacer thickness of 25, 50 and 100 μm, respectively. The CCFs in Fig. 1 (B-C) appear colored under white light illumination due to the presence of a partial photonic band gap. The CCF in Fig. 1 (D) appears white, suggesting that the larger particle size yields a less ordered structure lacking a well-defined photonic band gap. Fig. 1(E) compares the ICC membrane to a United States 25 cent coin. As shown in Fig. 1(F), when submerged in water the ICC membrane also appears colored, giving a qualitative indication of the regular pore structure of the membrane.

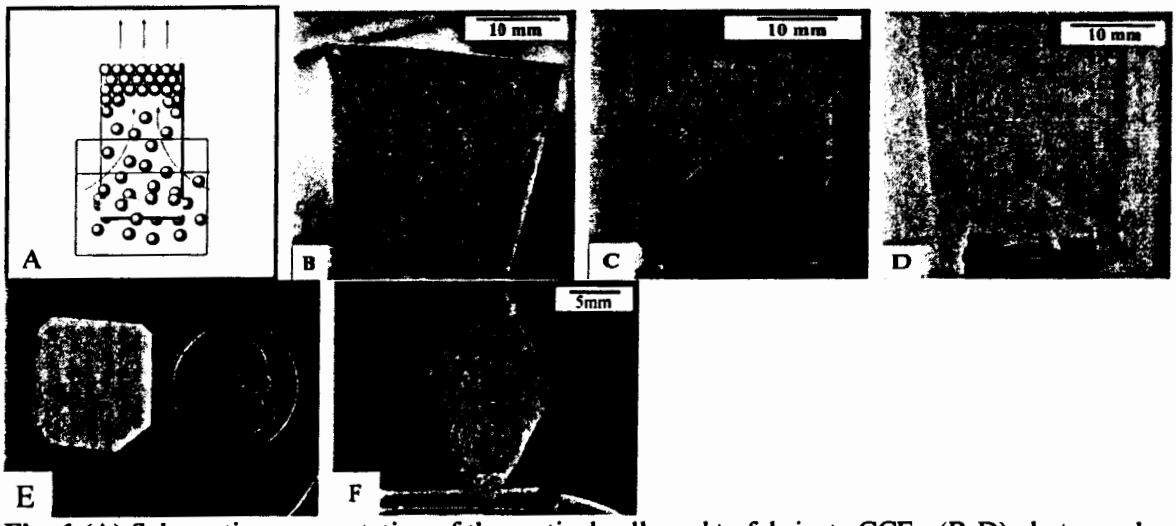

Fig. 1 (A) Schematic representation of the vertical cell used to fabricate CCFs. (B-D) photographs of CCFs fabricated from 423, 994 and 1998 nm spheres, respectively. (E) ICC membrane compared to United States 25 cent coin (approximate diameter 24 mm). (F)ICC membrane immersed in water appears colored.

Fig. 2 gives FESEM images of the CCFs and ICC membranes. Fig. 2 (A-C) shows the surface and a high magnification inset of 25 μm thick CCFs consisting of 423, 994, and 1998 nm

polystyrene spheres respectively. Since the 423 nm particles gave the most regular CCF, these films were studied in more detail. Fig. 2 (D-F) gives cross-sectional views of CCFs fabricated using 25, 50 and 100 μm thick spacers, fabricated with 423 nm particles. The FESEM images indicate that the film thickness is similar to the spacer thickness. Thus, the thickness of the CCF can be adjusted easily. Fig. 2 (G-H) show the top view and cross section of ICC membrane from 400 nm silicon dioxide sphere template. We can see from the SEM images that the pore size is similar to the size of the particles which is used for making CCF. The thickness of the ICC membrane can be made as thick as 100 μm.

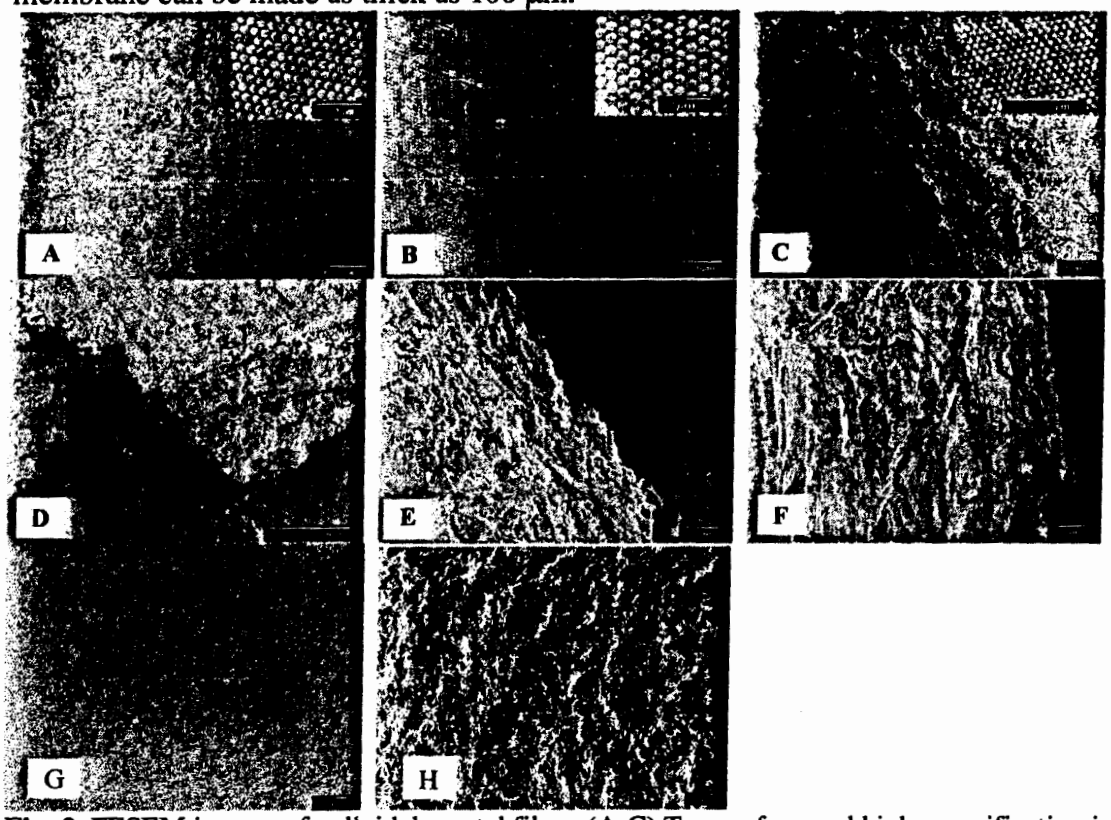

Fig. 2. FESEM images of colloidal crystal films. (A-C) Top surface and high magnification inset of CCFs fabricated using 423, 994 and 1998 nm spheres, respectively. (D-F) Cross-sectional images of CCFs assembled with 423 nm spheres with thicknesses of 25, 50 and 100 μm, respectively. (G) Top view of ICC membrane fabricated with 400 nm silicon dioxide spheres and 100 μm spacer. (H) Cross-section of (G).

4. Conclusion

A vertical cell assembly method has been developed for fabrication of large area CCFs with adjustable thickness. Assembly of CCFs using larger spheres results in less ordered structures. The ICC membranes resulting from the CCFs can be made as big as 500mm^2 and the thickness of ICC membranes can be as high as 100μm. The ICC membranes obtained from VC method are suitable for protein ultrafiltration and the protein tests of ICC membranes are under conducting in our lab.

Acknowledgements

Funding for this work was provided by the National Science Foundation, CBET 0651231.

References

[1] Waterhouse GIN, Waterland MR. Opal and inverse opals photonic crystals: fabrication and characterization. Polyhedron 2007; 26: 356-68.

[2] Lopez C. Materials aspects of photonic crystals. Adv Mater 2003; 15: 1679-704.

[3] Zakhidov AA, Baughman RH, Iqbal Z, Cui CX, Khayrullin I, Dantas SO, Marti I, Ralchenko VG. Carbon structures with three-dimensional periodicity at optical wavelengths. Science 1998; 282: 897-901.

[4] Weissman JM, Sunkar HB, Tse AS, Asher SA. Thermally switchable periodicities and diffraction from mesoscopically ordered materials. Science 1996; 274: 959-60.

[5] Xia YN, Gates B, Yin YD, Lu Y. Monodispersed colloidal spheres: old materials with new applications. Adv Mater 2000; 12: 693-713.

[6] Painter O, Lee RK, Scherer A, Yariv A, O'Brien JD, Dapkus PD, Kim I. Two-dimensional photonic band-gap defect mode laser. Science 1999; 284: 1819-21.

[7] Fudouzi H, Xia YN. Colloidal crystals with tunable colors and their use as photonic papers. Langmuir 2003; 19: 9653-60.

[8] Gates B, Yin Y, Xia Y. Fabrication and characterization of porous membranes with highly ordered three-dimensional periodic structures. Chem Mater 1999; 11: 2827-36.

[9] Ceska GW. The effect of carboxylic monomers on surfactant-free emulsion copolymerization. J Appl Polym Sci 1974; 18: 427-37.

[10] Stober W, Fink A, Bohn E. Controlled growth of monodisperse silica spheres in the micron size range. J. Colloid Interf Sci 1968; 26: 62-69.